J. Fluid Mech. (2007), *vol.* 579, *pp.* 413–443.
doi:10.1017/S002211200700537X Printed in the United Kingdom

A multi-mode approximation to wave scattering by ice sheets of varying thickness

L. G. BENNETTS, N. R. T. BIGGS AND D. PORTER

Department of Mathematics, The University of Reading, PO Box 220, Whiteknights, Reading, RG6 6AX, UK

(Received 19 June 2006 and in revised form 8 December 2006)

The problem of linear wave scattering by an ice sheet of variable thickness floating on water of variable quiescent depth is considered by applying the Rayleigh–Ritz method in conjunction with a variational principle. By using a multi-mode expansion to approximate the velocity potential that represents the fluid motion, Porter & Porter (*J. Fluid Mech.* vol. 509, 2004, p. 145) is extended and the solution of the problem may be obtained to any desired accuracy. Explicit solution methods are formulated for waves that are obliquely incident on two-dimensional geometry, comparisons are made with existing work and a range of new examples that includes both total and partial ice-cover is considered.

1. Introduction

The ability to determine the scattering of water waves by a floating ice sheet of varying thickness is both of physical importance and mathematically difficult. The energy carried by water waves is capable of travelling for long distances through an ice-covered region and is a factor in the fracturing of the ice. A thorough account of the mathematical and physical phenomena surrounding this topic may be found in Squire *et al.* (1995).

In this paper, the principal assumptions made are that linearized theory applies and that thin-elastic-plate theory can be used to model the ice-sheet, which supposes that it can be replaced by a homogeneous elastic plate whose physical parameters are considered known. This idealization of the ice includes the key property of flexure, but it ignores many others. Although, in the case of a floe of a semi-infinite extent, Balmforth & Craster (1999) showed that factors inherent in a model of 'non-thin' elastic plates, such as energy dissipation, friction and compression, are limited in their effect, it does not necessarily follow that a factor such as rotation, which is neglected in the thin-elastic-plate model, would not be significant in the case of a finite floe. In this work, we will retain the thin-elastic-plate model for simplicity; however, a model of 'non-thin' plates could be approached by a method similar to that which is outlined in this work. The question of the homogeneity of the ice also arises, particularly in respect of the stiffness of ice sheets containing keels or sails (downwards or upwards bulges) but, nonetheless, thin-plate theory is widely accepted as a good approximation.

The motion of the 'thin' elastic-plate is then taken in conjunction with the fluid beneath it and the coupled motion considered under linear and time harmonic conditions. The linear motion of a thin plate resting on fluid has also been investigated from the different perspective of VLFSs (very large floating structures), with one application to a proposed offshore runway (see, for example, Watanabe, Utsunomiya & Wang 2004).

An extensive catalogue of literature exists on the analysis of this form of wave scattering, with many different models and refinements possible. The assumption of uniformity of the plate's properties allows its effect to be confined to the equilibrium interface with the fluid, thus imposing a fourth-order condition to be satisfied at this fluid boundary. This is the source of the most significant difficulty that arises, in comparison to ordinary free-surface wave scattering. For this reason, many of the investigations that have been carried out have assumed constant thickness of the plate and a physically unrealistic zero draught, as the vertical fluid structure can then easily be analysed. However, the addition of submerged edges creates an extra source of scattering that may be of significance.

Currently, the analysis of two-dimensional problems has advanced to a stage at which restricted variations in the ice and bed geometries may be dealt with. Both Wang & Meylan (2002) and Belibassakis & Athanassoulis (2005) have allowed for finite length, zero draught plates on an otherwise free fluid surface of infinite extent over a bed that may vary its quiescent depth beneath the ice. Wang & Meylan (2002) obtain a solution by reducing the problem to a finite domain enclosed by a boundary (including the varying part of the bed and the lower surface of the plate) on which the normal derivative of the potential is expressed as a function of the potential itself. The problem is then solved numerically using a boundary-element method. Belibassakis & Athanassoulis (2005), on the other hand, use a variational principle and express the solution as an infinite series in the vertical eigenmodes, but add a further mode to allow for a non-horizontal bed. The resulting set of equations is then truncated and solved. Williams & Squire (2004) gave a solution procedure for an infinite fluid domain of constant depth, with a surface that is fully covered by ice whose upper surface is permitted to vary over a finite interval, although a zero draught is maintained. Their method of solution used a Green's function to produce an integral equation along the underside of the plate on the finite interval over which the upper surface varies, and this was solved numerically.

The study of three-dimensional problems has, thus far, been restricted to constant fluid depth and plate thickness with zero draught, and with simplifying assumptions about the horizontal shape of the ice. The case of a solitary circular plate resting on an infinite fluid surface with infinite depth was solved by Meylan & Squire (1996) by expressing the potential for the fluid motion as an integral posed on the underside of the plate, with conditions coupling it to the vertical displacement of the plate, and expanding the unknowns in terms of the horizontal eigenfunctions of the plate taken in isolation. Meylan (2002) extended this procedure to more general shapes of plate, although this extension requires the numerical determination of the required eigenfunction–eigenvalue pairs. Using the theory of solitary plates, Peter & Meylan (2004) have produced a study of the interaction of a finite number of plates, by implementing the ideas of Kagemoto & Yue (1986). By using a modal matching method, Peter, Meylan & Chung (2004) investigated the solitary circular plate problem over a finite fluid depth.

In a series of papers, Evans & Porter (2003, 2006) and Porter (2004) have examined the problem of cracks in ice sheets, determining the scattering properties of flexural–gravity waves by an arbitrary number of infinite or finite straight-line cracks in an otherwise uniform plate over a finite flat bed. This is achieved by deriving pairs of 'source functions' that act along the crack.

Other material on the general topic of water wave scattering by an elastic plate may be found in Balmforth & Craster (1999) and Squire *et al.* (1995).

In this paper, the work of Porter & Porter (2004, hereinafter referred to as PP), which is valid for ice and bed shapes restricted only by a requirement of slow variations, is

extended to remove this restriction. The addition of undulating topography is made with no extra algebraic or computational cost and its inclusion ensures that full generality of the geometry is allowed for in the model. Fundamental to this work was the derivation of a variational principle stating that the determination of the stationary point of a given functional is equivalent to solving the governing equations for linear scattering, in a three-dimensional setting and with full ice coverage. These equations include the conditions to be satisfied at corners in the ice and bed, as well as Laplace's equation in the fluid domain and boundary conditions at the bed and the water–ice interface. A further functional that allowed for partial ice covering was also developed. Seeking a stationary point of the functionals is reduced to a manageable level by an application of a form of the Rayleigh–Ritz method, in which the vertical fluid motion is restricted to a finite-dimensional space. By this means, the vertical spatial coordinate is removed by integration, a process which parallels the averaging that leads to thin-plate theory and gives an overall consistency to the model. The resulting simplified problem, involving only the horizontal coordinates, generates an approximation to the full linear solution. It is noted that the evaluation of particular quantities in PP overlooked certain terms and this is amended in this paper.

The vertical dependence used by PP was restricted to a single mode corresponding to the vertical eigenfunction that supports propagating waves when no variations in the ice thickness and bed topography are present. This idea extends the modified mild-slope approximation of Chamberlain & Porter (1995) for free-surface flows, and requires slow variations in the geometry. A numerical procedure was given by PP only in the case of two-dimensional motion.

The simple single-mode approximation of PP, with its unknown level of accuracy, can be extended to a multi-mode approximation, by including a finite number of the infinite set of eigenfunctions that support evanescent waves in the same way that the single mode supports propagating waves, and this procedure is carried out in the present work. The process of obtaining an approximation to the full linear solution to any desired degree of accuracy follows, with the variational principle generating increasingly improved approximations as more evanescent modes are included. For free-surface flows, the multi-mode approximation has been reappraised by Chamberlain & Porter (2006) in the light of the additional accuracy gained through the inclusion of a 'bed-mode', which was first proposed by Belibassakis & Athanassoulis (1999).

After summarizing the work covered by PP in § 2, including setting out the linear equations of motion in three-dimensions, with varying ice thickness and bed shapes, and reviewing the underlying theory, the full set of equations that govern the multi-mode approximation are determined in § 3. In § 4, we turn to the specific choice of modes suggested by PP and find that the evanescent modes have properties which compromise their use in some circumstances. An alternative expansion is suggested for situations in which the evanescent modes are not valid. In §§ 5–6, the multi-mode approximation is applied for two-dimensional geometry, but with obliquely incident waves; an analytic solution is given for uniform geometry, and this is used to create a numerical solution procedure for finite intervals of varying geometry surrounded by semi-infinite uniform states, either ice-covered or free-surface. Results are presented in § 7 to compare with the full linear solutions of previous authors, which act as a check on accuracy, before geometrical configurations which could not be investigated with previous methods are examined. Although the numerical work presented in this paper covers only a selection of two-dimensional situations, by developing theory that supports the approximation in a three-dimensional setting, we retain full generality of

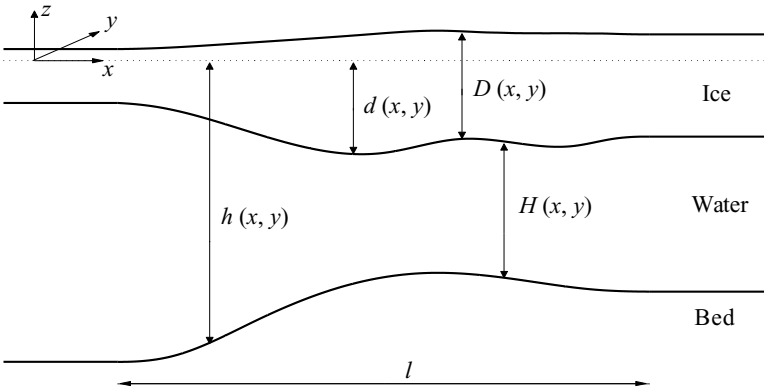

FIGURE 1. Two-dimensional cross-section of the geometry.

the model. This means that we will be able to deal with more complicated geometries (to appear in future work) without the need to redevelop the theory.

2. Preliminaries

We begin by stating the boundary-value problem derived by PP.

2.1. *The boundary-value problem*

A typical two-dimensional cross-section ($y=$constant) of the geometry is shown in figure 1. Fluid lies above a fixed impermeable bed located at $z=-h(x,y)$, where (x,y,z) are Cartesian coordinates with z directed vertically upwards and $z=0$ coinciding with the equilibrium surface of the fluid in the absence of ice. Initially, we consider the fluid surface to be wholly covered by ice, whose lower surface is located at $z=-d(x,y)$, and whose thickness is given by the function $D(x,y)$.

The fluid is assumed to be inviscid, incompressible and homogeneous, and in irrotational motion described by a velocity potential $\hat{\Phi}=\hat{\Phi}(x,y,z,t)$. Periodic time-dependence of the form $\mathrm{e}^{-\mathrm{i}\omega t}$, for given angular frequency ω, is assumed, so that the reduced velocity potential ϕ, such that $\hat{\Phi}(x,y,z,t)=\mathrm{Re}\{(g/\mathrm{i}\omega)\phi(x,y,z)\,\mathrm{e}^{-\mathrm{i}\omega t}\}$ where g is the acceleration due to gravity, can be introduced. The fluid motion induces periodic flexural oscillations in the ice sheet, and the position of its lower surface at time t can be written as $z=-d(x,y)+\eta(x,y)\,\mathrm{e}^{-\mathrm{i}\omega t}$. The amplitudes of the oscillations are assumed to be sufficiently small for linear theory to apply. Following PP, the reduced velocity potential ϕ and ice sheet elevation η then satisfy

$$\nabla^2\phi=0 \quad (-h<z<-d), \tag{2.1a}$$

$$\partial_z\phi+\nabla_h h\cdot\nabla_h\phi=0 \qquad (z=-h), \tag{2.1b}$$

$$(1-\alpha)\eta+\mathscr{L}\eta-\phi=0, \quad \nabla_h d\cdot\nabla_h\phi+\partial_z\phi=\kappa\eta \qquad (z=-d), \tag{2.1c}$$

where

$$\mathscr{L}\eta\equiv\nabla_h^2\big(\beta\nabla_h^2\eta\big)-(1-\nu)\big\{\big(\partial_x^2\beta\big)\big(\partial_y^2\eta\big)+\big(\partial_y^2\beta\big)\big(\partial_x^2\eta\big)-2(\partial_x\partial_y\beta)(\partial_x\partial_y\eta)\big\},$$
$$\nabla=(\partial_x,\partial_y,\partial_z), \quad \nabla_h=(\partial_x,\partial_y,0),$$

and

$$\alpha(x,y)=\kappa\rho_i D(x,y)/\rho_w, \quad \beta(x,y)=ED^3(x,y)/12\rho_w g(1-\nu^2).$$

The notation $\partial_x=\partial/\partial x$, and so on, is used throughout.

Here $\kappa = \omega^2/g$, ρ_w is the density of the fluid, ρ_i is the density of the ice, ν is Poisson's ratio, and E is Young's modulus. Unless otherwise stated, the parameters take the values $E = 5 \times 10^9$ Pa, $\rho_i = 922.5\,\mathrm{kg\,m^{-3}}$, $\rho_w = 1025\,\mathrm{kg\,m^{-3}}$, $\nu = 0.3$ and $g = 9.81\,\mathrm{m\,s^{-2}}$ (see, for example, Squire *et al.* 1995).

The mathematical description of the problem also requires some lateral conditions. In § 5, we will define radiation conditions for the two-dimensional problems for which we provide a numerical formulation in § 6 and results in § 7. However, as our initial concern is with the vertical structure of the motion, specific lateral conditions will not concern us for the present.

2.2. *Approximation of the vertical structure*

In order to solve the problem outlined in § 2.1, a Rayleigh–Ritz approximation is introduced so that the vertical structure of the motion is restricted to lie in a particular finite-dimensional set of functions. Taken in conjunction with a variational principle that will be described in § 2.3, this procedure provides a hierarchy of approximations to the solution of the boundary-value problem (2.1*a–c*) as the finite-dimensional set of functions is expanded. The functions that comprise the basis of this set are described as *vertical modes*, and the resulting approximation is termed a *multi-mode approximation* (MMA). This process provides a natural extension to the single-mode approximation of PP, in which the solitary mode is based on the vertical mode of the corresponding uniform geometry problem that supports wave propagation in the horizontal direction (see § 4 below). Thus, the PP approximation is

$$\phi(x, y, z) \approx \psi_0(x, y, z) = \varphi_0(x, y) \cosh k_0(z + h),$$

where $k_0 = k_0(x, y)$ is the unique positive, real root of the dispersion relation

$$(1 - \alpha + \beta k^4) k \tanh kH = \kappa, \tag{2.2}$$

with $H(x, y) = h(x, y) - d(x, y)$ (see figure 1) appearing for brevity.

The single-mode approximation of PP is based on an underlying assumption of the ice thickness and the bed topography varying slowly, and parallels the modified mild-slope approximation for free-surface fluid motions derived by Chamberlain & Porter (1995). Our objective is to extend the single-mode approximation to a multi-mode approximation, so that the full linear solution of the boundary-value problem may be obtained to any required degree of accuracy by taking a suitably large finite dimensional approximation in the vertical coordinate. This process corresponds to the extension to multiple modes for the free-surface problem described in, for example, Porter & Staziker (1995).

We introduce the MMA of dimension $N + 1$ defined by

$$\phi(x, y, z) \approx \psi_N(x, y, z) = \sum_{i=0}^{N} \varphi_i(x, y) w_i(x, y, z), \tag{2.3}$$

where the *natural modes* are given by

$$w_i(x, y, z) = \cosh k_i(z + h), \tag{2.4}$$

and the k_i are roots of the dispersion relation (2.2), taken in some logical order that will be described later. These roots may be regarded as functions of either the horizontal Cartesian coordinates x and y or the geometrical variables D, h and d. An alternative notation $w_i(x, y, z) \equiv W_i(D, h, d, z)$ will be used, when convenient,

to make explicit the dependence of the roots (and hence the vertical modes) on the geometrical variables. In intervals of uniform bed elevation and ice depth, the extra modes ($i = 1, \ldots, N$) support waves which decay in the horizontal direction. To complete the MMA it is necessary to calculate the amplitude functions $\varphi_i(x, y)$ ($i = 0, \ldots, N$).

2.3. *Variational principle*

Our approximation (2.3) has created the possibility of the inclusion of complex modes, so an amended version of the functional used in PP is required. We introduce the simply connected and bounded domain Ω in the plane $z = 0$, with boundary $\delta\Omega$, and suppose that the functions $\psi = \psi(x, y, z)$ and $\chi = \chi(x, y)$ are sufficiently differentiable for what follows. A simple modification of the argument of PP then shows that the required functional is $L_\Omega = L_\Omega(\psi, \chi) = 2\,\mathrm{Re}\,(\widetilde{L}_\Omega(\psi, \chi))$, where

$$2\widetilde{L}_\Omega(\psi, \chi) = \iint_\Omega \int_{-h}^{-d} (\nabla\psi)\cdot(\nabla\overline{\psi})\,\mathrm{d}z\,\mathrm{d}x\,\mathrm{d}y + \kappa \iint_\Omega (1-\alpha)\chi\overline{\chi} - 2\chi[\overline{\psi}]_{z=-d}\,\mathrm{d}x\,\mathrm{d}y$$
$$+\kappa \iint_\Omega \beta\left\{\left(\nabla_h^2\chi\right)\left(\nabla_h^2\overline{\chi}\right) - 2(1-\nu)\left(\left(\partial_x^2\chi\right)\left(\partial_y^2\overline{\chi}\right) - (\partial_x\partial_y\chi)(\partial_x\partial_y\overline{\chi})\right)\right\}\mathrm{d}x\,\mathrm{d}y,$$

with first variation $\delta L_\Omega = 2\,\mathrm{Re}\,(\delta H_\Omega)$, where

$$\delta H_\Omega = -\iint_\Omega \int_{-h}^{-d} \delta\overline{\psi}(\nabla^2\psi)\,\mathrm{d}z\,\mathrm{d}x\,\mathrm{d}y - \iint_\Omega [\delta\overline{\psi}(\nabla_h z\cdot\nabla_h\psi - \partial_z\psi)]_{z=-h}^{-d}\,\mathrm{d}x\,\mathrm{d}y$$
$$+\kappa \iint_\Omega \{(1-\alpha)\chi + \mathscr{L}\chi - [\psi]_{z=-d}\}\,\delta\overline{\chi} - \chi[\delta\overline{\psi}]_{z=-d}\,\mathrm{d}x\,\mathrm{d}y,$$

and where the variations are assumed to satisfy

$$\delta\psi = 0 \quad \text{on } \delta\Omega\times[-h,-d], \qquad \delta\chi = \delta\chi_x = \delta\chi_y = 0 \quad \text{on } \delta\Omega. \tag{2.5}$$

Hence, $\delta L_\Omega = 0$ at $\psi = \phi$, $\chi = \eta$ for any variations $\delta\psi$ and $\delta\chi$ satisfying (2.5) if and only if ϕ and η satisfy (2.1 *a–c*). (For details of the derivation of the original version of this result, see PP.) The solution of (2.1 *a–c*) can thus be found by locating the stationary point (ϕ, η) of $L_\Omega(\psi, \chi)$, and approximate solutions can be sought by approximating the stationary point of L_Ω.

2.3.1. *Ice-free regions*

If the ice only partially covers the surface of the fluid, then in ice-free regions the boundary-value problem (2.1*a–c*) and the associated variational principle L_Ω are modified accordingly. Suppose that $D = 0$ for $(x, y) \in \Omega$, then the first of the ice-sheet equations (2.1*c*) reduces to the condition $\eta = [\phi]_{z=0}$, and the functional L_Ω can be correspondingly amended to $L_\Omega^{(0)}(\psi) \equiv L_\Omega(\psi, [\psi]_{z=0})$. (On occasion, for clarity, the superscript (0) will be used to signify a quantity associated with the free surface.) The natural conditions of $\delta L_\Omega^{(0)} = 0$ with $\delta\psi = 0$ on $\delta\Omega\times[-h, 0]$ may then be deduced from (2.1*a–c*) to be

$$\nabla^2\phi^{(0)} = 0 \quad (-h < z < 0), \quad \partial_z\phi^{(0)} + \nabla_h h\cdot\nabla_h\phi^{(0)} = 0 \quad (z = -h), \quad \partial\phi_z^{(0)} = \kappa\phi^{(0)} \quad (z = 0).$$

As expected, these are the familiar equations describing linearized free-surface motions (see, for example, Porter & Staziker 1995).

2.4. *Jump conditions*

The set of equations (2.1*a–c*) apply only when the surrounding physical structure is suitably smooth. For instance, the first condition of (2.1*c*) requires the variation in the

ice thickness to be twice differentiable. At isolated locations where the geometry is not sufficiently differentiable, equivalent jump conditions replace the boundary-value problem. In fact, these jump conditions apply at all points in the domain Ω, regardless of whether the geometry is smooth or not and they may also be used for algebraic convenience (see, for example, § 6.1). The jump conditions are closely related to the interfacial conditions that are required to link ice-covered and ice-free regions.

Consider a curve Γ, say, which divides Ω into two domains Ω_+ and Ω_-. Assuming again that variations vanish on the lateral boundary of $\Omega_+ \cup \Omega_-$, there is a non-trivial contribution to $\delta(L_{\Omega_+} + L_{\Omega_-})$ on Γ, denoted by $G_\Gamma = 2\,\mathrm{Re}\,(\widetilde{G}_\Gamma)$, where

$$\widetilde{G}_\Gamma = \int_\Gamma \boldsymbol{n} \cdot \left\langle \int_{-h}^{-d} \delta\overline{\psi}(\nabla_h \psi)\,\mathrm{d}z + \kappa\left(\beta\nabla_h^2\chi\right)(\nabla_h\delta\overline{\chi}) - \kappa\delta\overline{\chi}\nabla_h\left(\beta\nabla_h^2\chi\right) - \kappa(1-\nu)\boldsymbol{g} \right\rangle \mathrm{d}s, \tag{2.6}$$

and

$$\begin{aligned}\boldsymbol{g} = &\left\{\beta\left[\left(\partial_y^2\chi\right)(\partial_x\delta\overline{\chi}) - (\partial_x\partial_y\chi)(\partial_y\delta\overline{\chi})\right] - \delta\overline{\chi}\left[(\partial_x\beta)\left(\partial_y^2\chi\right) - (\partial_y\beta)(\partial_x\partial_y\chi)\right]\right\}\boldsymbol{i}\\ &+\left\{\beta\left[\left(\partial_x^2\chi\right)(\partial_y\delta\overline{\chi}) - (\partial_x\partial_y\chi)(\partial_x\delta\overline{\chi})\right] - \delta\overline{\chi}\left[(\partial_y\beta)\left(\partial_x^2\chi\right) - (\partial_x\beta)(\partial_x\partial_y\chi)\right]\right\}\boldsymbol{j}.\end{aligned}$$

Here, $\langle\chi\rangle = \chi_+ - \chi_-$ denotes the jump in χ across Γ, with $\chi_\pm$ denoting the limiting value from $\Omega_\pm$, s denotes arclength on Γ, $\boldsymbol{n}$ is the unit normal to Γ (oriented from Ω_+ into Ω_- for definiteness), and $\boldsymbol{i}$ and $\boldsymbol{j}$ are the unit vectors in the x- and y-directions, respectively. In order that $\delta(L_{\Omega_+} + L_{\Omega_-}) = 0$, $\widetilde{G}_\Gamma$ is required to vanish at a stationary point.

2.4.1. *Connected ice boundary*

If the domains $\Omega_\pm$ are both completely ice-covered, then the essential conditions

$$\langle\langle\psi\rangle\rangle = \langle\chi\rangle = \langle\boldsymbol{n}\cdot\nabla_h\chi\rangle = 0$$

are imposed, where $\langle\langle\psi\rangle\rangle = \psi_+ - \psi_-$ denotes the jump across $\Gamma \times [-h, -d]$. These conditions represent continuity of fluid pressure, and continuity of ice-sheet displacement and velocity across Γ, respectively. From (2.6), we then deduce the set of natural conditions

$$\langle\langle\boldsymbol{n}\cdot\nabla_h\phi\rangle\rangle = \langle\mathfrak{M}\eta\rangle = \langle\mathfrak{S}\eta\rangle = 0 \tag{2.7}$$

which must hold for stationary points $\psi = \phi$ and $\chi = \eta$ of $\delta(L_{\mathscr{D}_+} + L_{\mathscr{D}_-}) = 0$, where

$$\begin{aligned}\mathfrak{M}\eta &\equiv \beta\nabla_h^2\eta - (1-\nu)\beta(\partial_s^2\eta + \Theta'(\partial_n\eta)),\\ \mathfrak{S}\eta &\equiv \partial_n(\beta\nabla_h^2\eta) - (1-\nu)\{(\partial_s^2\eta + \Theta'(\partial_n\eta))(\partial_n\beta)\\ &\quad -2((\partial_s\partial_n\eta) - \Theta'(\partial_s\eta))(\partial_s\beta) - \beta\partial_s((\partial_s\partial_n\eta) - \Theta'(\partial_s\eta))\}.\end{aligned}$$

Here $\partial_n = \boldsymbol{n}\cdot\nabla_h$, $\partial_s = \boldsymbol{s}\cdot\nabla_h$ with $\boldsymbol{s}$ a unit vector tangential to Γ, and $\boldsymbol{n}$ has direction cosines $(\cos\Theta(s), \sin\Theta(s), 0)$ with respect to the Cartesian frame.

Finally, the derivation of (2.7) also introduces the point condition

$$(\partial_s\partial_n\eta) - \Theta'(\partial_s\eta) \equiv \partial_n\partial_s\eta = 0,$$

which holds at the ends of Γ (see PP).

The natural conditions (2.7) ensure continuity of horizontal fluid velocity, and bending moment and shearing stress of the ice sheet across Γ, respectively.

2.4.2. *Water–ice interface*

If a portion of the domain Ω is free of ice, then jump conditions between the ice-covered and ice-free regions must be imposed at the interface. As before, we

write $\Omega = \Omega_- \cup \Omega_+$, but now suppose that the region Ω_- is ice-free. The contribution along Γ to $\delta(L^{(0)}_{\Omega_-} + L_{\Omega_+})$, where as before $L^{(0)}_{\Omega_-}(\psi) \equiv L_{\Omega_-}(\psi, [\psi]_{z=0})$, is denoted by $2\,\mathrm{Re}\,(\widetilde{G}^{(0)}_{\Gamma})$, where

$$\widetilde{G}^{(0)}_{\Gamma} = \int_{\Gamma} \boldsymbol{n} \cdot \left\{ \int_{-h}^{-d_+} \delta\overline{\psi}_+ (\nabla_h \psi_+) \mathrm{d}z - \int_{-h}^{0} \delta\overline{\psi}^{(0)}_- \left(\nabla_h \psi^{(0)}_-\right) \mathrm{d}z \right.$$
$$\left. + \kappa \left(\beta \nabla_h^2 \chi_+\right)(\nabla_h \delta\overline{\chi}_+) - \kappa\, \delta\overline{\chi}_+ \nabla_h \left(\beta \nabla_h^2 \chi_+\right) - \kappa(1-\nu)\boldsymbol{g} \right\} \mathrm{d}s.$$

Although it is possible to derive the correct jump conditions by setting $\widetilde{G}^{(0)}_{\Gamma} = 0$, with the essential condition $\langle\langle \psi \rangle\rangle = 0$, we will rather make a modification as it is anticipated that this essential continuity is precluded by the jump in the natural modes across the interface Γ, caused by the discontinuity in D in moving from free-surface to ice-covered states (assuming that $D \neq 0$ at the edge of the floe). Following PP, the problematic essential condition, $\langle\langle \psi \rangle\rangle = 0$, which requires continuity of the modes across Γ, is removed by the introduction of the functional

$$I_{\Gamma}(\psi, u) = \frac{1}{2} \int_{\Gamma} \int_{-h}^{-d_+} \left\{ \left(\psi_+ - \psi^{(0)}_-\right)\overline{u} + \left(\overline{\psi}_+ - \overline{\psi}^{(0)}_-\right) u \right\} \mathrm{d}z\, \mathrm{d}s,$$

where u is an auxiliary function. The functional I_{Γ} ensures coupling of the fluid motion between the free-surface and ice-covered states, which is lost by the removal of $\langle\langle \psi \rangle\rangle = 0$. Now, enforcing $\delta(L^{(0)}_{\Omega_-} + L_{\Omega_+} - I_{\Gamma}) = 0$, and assuming that χ and $\boldsymbol{n} \cdot (\nabla_h \chi)$ are bounded at the ice-edge, results in natural conditions:

$$\left.\begin{array}{c} \mathfrak{M}\eta_+ = \mathfrak{S}\eta_+ = 0 \quad (x, y \in \Gamma), \\ \boldsymbol{n} \cdot \nabla_h \phi_+ = \boldsymbol{n} \cdot \nabla_h \phi^{(0)}_- = u \\ \phi_+ = \phi^{(0)}_- \end{array}\right\} \quad (x, y \in \Gamma, -h < z < d_+), \tag{2.8}$$

and

$$\boldsymbol{n} \cdot \nabla_h \phi^{(0)}_- = 0 \quad (x, y \in \Gamma, -d_+ < z < 0), \tag{2.9}$$

to be satisfied by the stationary point. The transferral of $\langle\langle \phi \rangle\rangle = 0$ from an essential to a natural condition ensures that a consistent natural MMA may be applied throughout a domain of only partial ice-cover. The natural conditions that we have derived are generalizations of the matching conditions used, for example, in the eigenfunction matching methods employed by Fox & Squire (1994) and Peter *et al.* (2004).

Slightly modified versions of I_{Γ} may be used to deal with more general discontinuities in the trial space, caused by discontinuities in the surrounding geometry or otherwise. In particular, this modification will be required in § 7, where a situation arises in which the MMA is applied over point discontinuities in the ice thickness. It is noted, however, that the validity of all essential conditions applied should be carefully considered in the context of the problem, wherever discontinuities exist.

For the sake of algebraic clarity, throughout §§ 3–6, it will be assumed that the only discontinuities in the geometry are caused by the edge of an ice floe.

3. The multi-mode approximation

We now examine the effect of inserting the approximation (2.3), for the reduced velocity potential, into the variational principle introduced in § 2. In contrast, the

displacement function is only indirectly approximated. To retain full generality, we only assume the form of the approximation (2.3), leaving the specific choice of the vertical modes w_i until a later stage.

Substituting the expansion ψ_N from (2.3) into the functional L_Ω and enforcing the stationary condition $\delta L_\Omega(\psi_N, \chi) = 0$ gives

$$-\sum_{j=0}^{N} \iint_\Omega \delta\overline{\varphi}_j \left\{ \int_{-h}^{-d} \overline{w}_j \sum_{i=0}^{N} \nabla^2(\varphi_i w_i)\,\mathrm{d}z + \kappa\chi\,[\overline{w}_j]_{z=-d} + \left[\overline{w}_j \sum_{i=0}^{N} \{\nabla_h z\cdot\nabla_h(\varphi_i w_i) - \varphi_i(\partial_z w_i)\} \right]_{z=-h}^{-d} \right\} \mathrm{d}x\,\mathrm{d}y + \kappa \iint_\Omega \delta\overline{\chi} \left\{ (1-\alpha)\chi + \mathscr{L}\chi - \sum_{i=0}^{N} \varphi_i [w_i]_{z=-d} \right\} \mathrm{d}x\,\mathrm{d}y = 0.$$

It follows that the functional $L_\Omega(\psi, \chi)$ is stationary with respect to variations $\delta\psi$ and $\delta\chi$ satisfying (2.5) provided that

$$\int_{-h}^{-d} \overline{w}_j \sum_{i=0}^{N} \nabla^2(\varphi_i w_i)\,\mathrm{d}z + \kappa\chi\,[\overline{w}_j]_{z=-d} + \left[\overline{w}_j \sum_{i=0}^{N} \{\nabla_h z\cdot\nabla_h(\varphi_i w_i) - \varphi_i(\partial_z w_i)\} \right]_{z=-h}^{-d} = 0 \tag{3.1}$$

for $j = 0, \ldots, N$, and

$$(1-\alpha)\chi + \mathscr{L}\chi - \sum_{i=0}^{N} \varphi_i [w_i]_{z=-d} = 0. \tag{3.2}$$

Equation (3.1) may be simplified, by using the identity

$$\int_{-h}^{-d} \overline{w}_j \nabla_h^2(w_i\varphi_i)\,\mathrm{d}z = \int_{-h}^{-d} \overline{w}_j(\nabla_h w_i)\cdot(\nabla_h\varphi_i) - (\nabla_h\overline{w}_j)\cdot(w_i\nabla_h\varphi_i + \varphi_i\nabla_h w_i)\,\mathrm{d}z - \left[\overline{w}_j\nabla_h z\cdot\nabla_h(w_i\varphi_i)\right]_{z=-h}^{-d} + \nabla_h\cdot\left\{ \int_{-h}^{-d} \overline{w}_j w_i\,\mathrm{d}z \right\}\nabla_h\varphi_i + \left\{ \nabla_h\cdot \int_{-h}^{-d} \overline{w}_j(\nabla_h w_i)\,\mathrm{d}z \right\}\varphi_i,$$

to

$$\sum_{i=0}^{N} \{\nabla_h\cdot(a_{j,i}\nabla_h\varphi_i) + \widetilde{\boldsymbol{d}}_{j,i}\cdot(\nabla_h\varphi_i) + b_{j,i}\varphi_i\} + \kappa\chi\,[\overline{w}_j]_{z=-d} = 0, \tag{3.3}$$

where

$$a_{j,i} = \int_{-h}^{-d} \overline{w}_j w_i\,\mathrm{d}z, \quad \widetilde{\boldsymbol{d}}_{j,i} = \int_{-h}^{-d} \overline{w}_j(\nabla_h w_i) - w_i(\nabla_h\overline{w}_j)\,\mathrm{d}z,$$

and

$$b_{j,i} = \int_{-h}^{-d} \overline{w}_j\left(\partial_z^2 w_i\right)\mathrm{d}z - [\overline{w}_j(\partial_z w_i)]_{z=-h}^{-d} + \nabla_h\cdot\int_{-h}^{-d} \overline{w}_j(\nabla_h w_i)\,\mathrm{d}z - \int_{-h}^{-d} (\nabla_h\overline{w}_j)\cdot(\nabla_h w_i)\,\mathrm{d}z.$$

Equations (3.2) and (3.3) thus govern the MMA. For convenience, the system of equations (3.3) will often be written as the more compact matrix equation

$$\nabla_h\cdot(\boldsymbol{A}\nabla_h\boldsymbol{\Phi}_N) + \widetilde{\boldsymbol{D}}\cdot(\nabla_h\boldsymbol{\Phi}_N) + \boldsymbol{B}\boldsymbol{\Phi}_N + \kappa\chi\overline{\boldsymbol{C}}\boldsymbol{f} = 0, \tag{3.4}$$

where $\boldsymbol{\Phi}_N = (\varphi_0, \ldots, \varphi_N)^T$, $\boldsymbol{C} = \mathrm{diag}\{[w_0]_{z=-d}, \ldots, [w_N]_{z=-d}\}$, and $\boldsymbol{f} = (1, \ldots, 1)^T$, while $A_{j,i} = a_{j-1,i-1}$, $B_{j,i} = b_{j-1,i-1}$ and $\widetilde{\boldsymbol{D}}_{j,i} = \widetilde{\boldsymbol{d}}_{j-1,i-1}$ for $i, j = 1, \ldots, N+1$. Note that $\widetilde{\boldsymbol{d}}_{i,j} = -\overline{\widetilde{\boldsymbol{d}}}_{j,i}$ and hence that $\widetilde{\boldsymbol{d}}_{i,i} = 0$ for real-valued modes.

For practical purposes, the coefficients can be written as

$$\widetilde{\boldsymbol{d}}_{j,i} = \big(P^{(D)}_{j,i} - \overline{P}^{(D)}_{i,j}\big)\nabla_h D + \big(P^{(h)}_{j,i} - \overline{P}^{(h)}_{i,j}\big)\nabla_h h + \big(P^{(d)}_{j,i} - \overline{P}^{(d)}_{i,j}\big)\nabla_h d, \tag{3.5}$$

where, in terms of the inner-product notation

$$(u, v) = \int_{-h}^{-d} u\overline{v}\,\mathrm{d}z,$$

we have written

$$P^{(X)}_{j,i} = (\partial_X W_i, W_j) \quad \text{for } X = D, h, d,$$

and

$$\begin{aligned} b_{j,i} = {} & \int_{-h}^{-d} \overline{w}_j\big(\partial_z^2 w_i\big)\,\mathrm{d}z - [\overline{w}_j(\partial_z w_i)]^{-d}_{z=-h} + P^{(D)}_{j,i}\nabla_h^2 D + P^{(h)}_{j,i}\nabla_h^2 h + P^{(d)}_{j,i}\nabla_h^2 d \\ & + Q^{(D,D)}_{j,i}(\nabla_h D)^2 + Q^{(h,h)}_{j,i}(\nabla_h h)^2 + Q^{(d,d)}_{j,i}(\nabla_h d)^2 \\ & + \big(Q^{(D,h)}_{j,i} + Q^{(h,D)}_{j,i}\big)(\nabla_h D)\cdot(\nabla_h h) + \big(Q^{(D,d)}_{j,i} + Q^{(d,D)}_{j,i}\big)(\nabla_h D)\cdot(\nabla_h d) \\ & + \big(Q^{(d,h)}_{j,i} + Q^{(h,d)}_{j,i}\big)(\nabla_h d)\cdot(\nabla_h h), \end{aligned} \tag{3.6}$$

with

$$Q^{(X,Y)}_{j,i} = \partial_Y(\partial_X W_i, W_j) - (\partial_Y W_i, \partial_X W_j) \quad \text{for } X, Y = D, h, d.$$

We note here that the evaluation of the coefficients in PP omitted certain terms in (3.5)–(3.6) relating to d. The approximation of PP thus unwittingly created equivalence classes of geometries, related by a shared ice thickness $D(x)$ and fluid depth $H(x)$. In particular, this led to spurious results for non-constant d. The introduction of the missing terms establishes the position of the horizontal water–ice interface d, so that the approximation is uniquely defined by the chosen geometry.

Equations (3.2) and (3.3) only hold in regions where h, d and D are differentiable. Where this is not the case, these equations are replaced by equivalent jump conditions.

3.1. *Jump conditions at a connected ice boundary*

Making the assumption that, across a contour Γ that separates the two ice-covered domains $\Omega_\pm$, the ice and fluid boundaries are continuous and that the ice is connected, the contribution to $\delta(L_{\Omega_-} + L_{\Omega_+})$ is twice the real part of

$$\sum_{j=0}^{N}\sum_{i=0}^{N}\int_\Gamma \left\langle \delta\overline{\varphi}_j \int_{-h}^{-d} \overline{w}_j \boldsymbol{n}\cdot\nabla_h(\varphi_i w_i)\,\mathrm{d}z \right\rangle \mathrm{d}s. \tag{3.7}$$

Taking the essential condition

$$\langle\langle \boldsymbol{\Phi}_N \rangle\rangle = \boldsymbol{0}, \quad ((x, y) \in \Gamma, z \in (-h, -d)), \tag{3.8}$$

which implies $\langle\langle \psi_N \rangle\rangle = 0$, and setting (3.7) to zero, leads to the jump condition

$$\langle(\boldsymbol{n}\cdot\boldsymbol{A}(\nabla_h\boldsymbol{\Phi}_N)_+ + \boldsymbol{J}\boldsymbol{\Phi}_N)\rangle = 0, \tag{3.9}$$

in which

$$J_{m+1,n+1} = \int_{-h}^{-d} \overline{w}_m \boldsymbol{n}\cdot\nabla_h w_n\,\mathrm{d}z \quad (m, n = 0, \ldots, N).$$

Notice that $J_{m+1,n+1} = P^{(D)}_{m,n}\boldsymbol{n}\cdot\nabla_h D + P^{(h)}_{m,n}\boldsymbol{n}\cdot\nabla_h h + P^{(D)}_{m,n}\boldsymbol{n}\cdot\nabla_h d$. The conditions on the indirectly approximated vertical displacement of the ice remain as $\langle\mathfrak{M}\chi\rangle = \langle\mathfrak{S}\chi\rangle = 0$, where the essential conditions $\langle\chi\rangle = \langle\boldsymbol{n}\cdot\nabla_h\chi\rangle = 0$ are applied.

3.2. *Jump conditions at an ice–water boundary*

Following the discussion of § 2.4.2, for contours Γ that define an ice–water boundary, we drop the requirement that $\langle\langle\psi_N\rangle\rangle = 0$, and instead set $\delta(L^{(0)}_{\Omega_-} + L_{\Omega_+} - I_\Gamma) = 0$ along Γ.

It is necessary to approximate the auxiliary function u in a manner consistent with the MMA ψ_N. We write

$$u \approx \sum_{i=0}^{N} u_i(x, y)v_i(x, y, z),$$

where the modes v_i will be left unspecified for the present.

The contribution to the first variation of the functional $L^{(0)}_{\Omega_-} + L_{\Omega_+} - I_\Gamma$ along Γ of the directly approximated functions is twice the real part of

$$\sum_{j=0}^{N}\sum_{i=0}^{N}\int_\Gamma\left\{\int_{-h}^{-d}(\delta\overline{\varphi}_j\overline{w}_j)_+\{\boldsymbol{n}\cdot\nabla_h(w_i\varphi_i)_+ - u_iv_i\} - \delta\overline{u}_j\overline{v}_j(w_i\varphi_i)_+\,\mathrm{d}z\right.$$
$$\left. - \int_{-h}^{0}(\delta\overline{\varphi}_j\overline{w}_j)^{(0)}_-\boldsymbol{n}\cdot(\nabla_h w_i\varphi_i)^{(0)}_-\,\mathrm{d}z + \int_{-h}^{-d}\left\{(\delta\overline{\varphi}_j\overline{w}_j)^{(0)}_- u_iv_i + \delta\overline{u}_j\overline{v}_j(w_i\varphi_i)^{(0)}_-\right\}\mathrm{d}z\right\}\mathrm{d}s.$$

From this, we deduce the natural conditions

$$(\overline{\boldsymbol{V}}^T\boldsymbol{\Phi}_N)_+ = (\overline{\boldsymbol{V}}^T\boldsymbol{\Phi}_N)_-, \tag{3.10}$$

and

$$\boldsymbol{n}\cdot(\boldsymbol{A}\nabla_h\boldsymbol{\Phi}_N)_\pm + (\boldsymbol{J}\boldsymbol{\Phi}_N)_\pm = V_\pm\boldsymbol{u}, \tag{3.11}$$

where

$$V_{j+1,i+1} = \int_{-h}^{-d}\overline{w}_jv_i\,\mathrm{d}z \quad (i, j = 0, \ldots, N),$$

and $\boldsymbol{u} = (u_0, \ldots, u_N)^T$. It is now clear that $\boldsymbol{u}$, which is superfluous to the final approximation, may be eliminated from (3.11) to leave the condition

$$(\boldsymbol{V}_+)^{-1}((\boldsymbol{n}\cdot\boldsymbol{A}\nabla_h\boldsymbol{\Phi}_N)_+ + (\boldsymbol{J}\boldsymbol{\Phi}_N)_+) = (\boldsymbol{V}_-)^{-1}(\boldsymbol{n}\cdot(\boldsymbol{A}\nabla_h\boldsymbol{\Phi}_N)_- + (\boldsymbol{J}\boldsymbol{\Phi}_N)_-), \tag{3.12}$$

where we have assumed the matrices $\boldsymbol{V}_\pm$ to be invertible.

Basing our selection on (2.8), we choose to set the modes $v_i(x, y, z) = [w_i(x, y, z)]_{(x,y)\in\Gamma_+}$ for the computation of results in this paper. It is noted that there may exist a more judicious choice. It should also be noted that this choice differs in the $N = 0$ case from that of PP, who based their selection of v_0 on an average across the interface. However, this produced an approximation that could not be expected to span the appropriate space if extended to an MMA.

The conditions on the vertical displacement again are not changed from the exact conditions, so that $\mathfrak{M}\chi_+ = \mathfrak{S}\chi_+ = 0$ holds at Γ.

4. Choice of approximation

The solution of the full linear problem, when D, h and d are all constant, has the form

$$\phi(x, y, z) = \sum_{i=0}^{\infty} \phi_i(x, y) \cosh k_i(z + h) \tag{4.1}$$

(for details see Evans & Porter 2003). This leads us to conjecture that the finite sum

$$\psi_N(x, y, z) = \sum_{i=0}^{N} \varphi_i(x, y) \cosh\{k_i(x, y)(z + h(x, y))\}$$

will provide a good approximation to the exact solution ϕ in regions where all fluid and ice boundaries are fully variable.

It is expected that a relatively small number of the most significant modes will provide a good approximation. However, the nature of the roots k_i, as D, h and d vary, is not always conducive to such an approximation.

We remark here that we do not non-dimensionalize the variables, which would obscure the significance of the various quantities in the ice thickness. Appropriate non-dimensionalizations are given by other authors, for example Fox (2001) and Williams & Squire (2004).

4.1. *Roots of the dispersion relation*

It has already been stated that there is only one positive real root of the dispersion relation (2.2) and it can be shown that this root lies in the interval $(0, \mathscr{U})$, where $\mathscr{U} = \max\{\kappa \coth(\kappa), \kappa H^{-1}, (\alpha\beta^{-1})^{1/4}\}$, and it is therefore easily found numerically.

Note at this point that, for any root k of the dispersion relation, there always exists another root $-k$. As each $\pm k$ pair contribute the same vertical mode we can concentrate our search for roots to the complex domain $k = \mathrm{Re}^{\mathrm{i}\theta} \in \mathbb{C}$ such that $R > 0$, and $0 \leqslant \theta < \pi$. It is also obvious that, as the coefficients involved in the dispersion relation are real, if we find a complex root then its conjugate is also a root.

Let us now consider the possibility of purely imaginary roots. If we choose to write the roots as $k = \mathrm{i}\sigma$, such that $\sigma > 0$, then the dispersion relation may be written

$$(1 - \alpha + \beta\sigma^4)\sigma = -\kappa \cot(\sigma H). \tag{4.2}$$

This expression makes it clear that at least one root lies on each branch of $\cot(\sigma H)$, that is, in the interval (l_{n-1}, l_n), such that $l_n = n\pi/H$, and that $\sigma_n \to l_n$ as $n \to \infty$.

Application of the principle of the argument (see Evans & Davies 1968) proves that there exist two further roots, for which there are two possibilities: the combination of the various parameters may produce complex roots that are symmetric about the imaginary axis or two extra purely imaginary roots that occupy the same branch of $\cot(\sigma H)$, so that, on that branch only, there are three roots. If the ice thickness and fluid depth are allowed to vary continuously between states where these roots bifurcate from complex to purely imaginary or vice versa, then there is inevitably a point at which the roots coalesce, forming a double (or, possibly, a treble) root.

The creation of a multiple root is controlled by the value $C = 2^8(1 - \alpha)^5/\kappa^4\beta$ and the fluid depth H. There exist values C_n $(n = 0, \ldots)$ of C, such that $C_{n+1} < C_n$ $(n \geqslant 0)$ and with $C_0 \approx 1.3 \times 10^{-3}$, such that for $C \leqslant C_n$, multiple roots will exist in the interval (l_n, l_{n+1}) for some values of H. This information is also deduced by Williams (2006) and the above value of C_0 is consistent with the value given in that work. We may therefore select, for example, $\omega = 3.00\,\mathrm{rad\,s^{-1}}$, $D = 1.21\,\mathrm{m}$ and $H = 22.9\,\mathrm{m}$ as physically

realistic parameters (see Balmforth & Craster 1999) for which a multiple root occurs in (l_0, l_1), where $l_0 = 0$. The possibility of creating multiple roots in subsequent intervals would require the use of unrealistic parameter values, that is, extremely thick ice and small wave period. Further discussion on the behaviour of the roots of the dispersion relation can be found in Williams (2006). It is further noted that the dispersion relation (2.2) has appeared in the work of other authors who did not detect (or, at least, report) the possibility of a configuration of the roots other than one in which a complex symmetric pair exist.

At the point at which a multiple root is created, it can be shown that the paths of the constituent roots are non-differentiable functions (with respect to all independent variables). In fact, it can be shown that, in the neighbourhood of a bifurcation, the derivative (with respect to all independent variables) of a bifurcating root is unbounded. However, in order to implement the MMA, we must differentiate the natural modes w_i, which implicitly requires the differentiability of the roots k_i. The problem created by bifurcations can, to some extent, be offset by the linear dependence of the natural modes that will be discussed in § 4.2. However, there remain situations in which we are unable to use the natural MMA as it stands. Although there exist avenues through which the bifurcating modes may be modified to allow their retention, these methods are cumbersome, and the problem is rather avoided simply by approximating the solution using a different expansion set; an example of this is given in § 7. We note that the complication presented by bifurcating roots is simply an artifice of the method and does not represent a physical process.

The roots of the dispersion relation will be denoted: k_0 for the unique positive, real root; $k_i = i\sigma_i$ $(i \geqslant 1)$ for the purely imaginary roots, where $\sigma_{i+1} > \sigma_i > 0$ and $k_{-i} = \mu_i$ $(i = 1, 2)$ will refer to the complex roots. Correspondingly, the natural approximation (2.3) is rewritten as

$$\psi_N(x, y, z) = \sum_{i=-2}^{N} \varphi_i(x, y) w_i(x, y, z). \tag{4.3}$$

4.2. *Linear dependence*

The primary reason that we require the roots of the dispersion relation is to construct the modes (2.4) on which the natural approximation is built. Here we mimic a result that can be found in the Appendix of Evans & Porter (2003), but make explicit an important implication of the result concerning the linear dependence of our trial functions.

Consider the integral

$$\frac{1}{2\pi \mathrm{i}} \oint \frac{f_a(\tau)}{\mathfrak{K}(\tau)} \cosh \tau(z + h) \, \mathrm{d}\tau,$$

integrated about a circle centred at the origin, of radius R, where

$$\mathfrak{K}(\tau) = (1 - \alpha + \beta\tau^4)\tau \sinh(\tau H) - \kappa \cosh(\tau H),$$

is an even function, and f_a is a currently unspecified odd function that is holomorphic in the circle about which we are integrating.

Assuming that the parameter set used does not give rise to a double root (i.e. a point at which the μ_i $(i = 1, 2)$ coalese) application of the residue theorem gives

$$2 \sum_{n=-2}^{N} \frac{f_a(k_n)}{\mathfrak{K}'(k_n)} \cosh k_n(z + h) = B_R,$$

where B_R is the contribution from the boundary, and we are supposing that only the roots $\pm k_n$ $(n=-2,\ldots,N)$ are contained in the circle.

Now, suppose that $\tau = R\mathrm{e}^{\mathrm{i}\theta}$, and f_a is selected such that the contribution from the boundary decays as $R\to\infty$, then

$$2\sum_{n=-2}^{\infty}\frac{f_a(k_n)}{\mathfrak{K}'(k_n)}\cosh k_n(z+h)=0. \tag{4.4}$$

This result tells us that there exists a subset of the natural modes

$$\{\cosh k_n(z+h)\}\quad (n=-2,-1,0,1,\ldots) \tag{4.5}$$

that spans the same space. The degree by which we may reduce the natural set (4.5) depends on how many linearly independent ways we may select the function f_a.

It may easily be deduced that the only admissable f_a are such that $f_a(\tau)=a_1\tau+a_3\tau^3$, for constants a_1 and a_3. Therefore, $f_a(k_n)=k_n$ and $f_a(k_n)=k_n^3$ are the only two linearly independent possibilities.

In terms of the uniform problem, we have shown that for any distribution of the roots of (2.2), in which the roots do not coincide, the vertical motion may be expressed by any subset of (4.5) with two members removed. The horizontal waves corresponding to the vertical modes that are no longer present are then redistributed amongst those remaining vertical modes. In situations in which any of the roots of (2.2) coincide, extra functions will arise in (4.4) in place of the repeated modes.

Note that, the coefficients $f_a(k_n)/\mathfrak{K}'(k_n)$ decay as $n\to\infty$, and hence only a few of the natural modes are important in this linear-dependence issue. Although we work only with a finite number, N, of vertical modes, it can therefore be expected that numerical problems will be experienced for small N, if the natural approximation is applied in its current form (4.3), but that nothing will be lost from the approximation if two of the significant modes are removed.

4.3. *The natural approximation*

As indicated in § 4.2, it is possible to use our two degrees of freedom to reduce the problems created by possible bifurcations. That is, if only two roots bifurcate as the parameters vary, then these roots may be discarded, leaving a viable approximation. However, if any more than two roots bifurcate then the natural MMA must be abandoned. If no bifurcations occur, and complex roots are present, then we choose to remove the modes corresponding to these roots as this affords the advantage that the remaining trial functions are real-valued. When no complex roots exist, we arbitrarily select our purely imaginary roots such that only one from each interval (l_{n-1}, l_n) is used.

Given what has just been said, the natural approximation is redefined as

$$\psi_N(x,y,z)=\sum_{i=0}^{N}\varphi_i(x,y)w_i(x,y,z).$$

It is clear that the degenerate case $N=0$ coincides with the approximation employed by PP, except where there are water–ice junctions for which we have modified the jump conditions used in the earlier paper.

4.4. *Coefficients for the natural modes*

Having chosen a suitable expansion set, we can evaluate the coefficients arising in the equations that govern the approximation, which were defined at the beginning of § 3.

We find that

$$a_{j,i} = \begin{cases} (k_i \sinh(k_i H)\cosh(k_j H) - k_j \sinh(k_j H)\cosh(k_i H))/\left(k_i^2 - k_j^2\right) & (i \neq j), \\ (\sinh(2k_i H) + 2k_i H)/4k_i & (i = j). \end{cases} \tag{4.6}$$

Some simplification of the $b_{j,i}$ is afforded by the properties $[\partial_z w_i]_{z=-h} = 0$ and $\partial_z^2 w_i = k_i^2 w_i$ of the natural modes, so that

$$\begin{aligned} b_{j,i} = {} & k_i^2 a_{j,i} - k_i \sinh(k_i H)\cosh(k_j H) + P_{j,i}^{(D)} \nabla_h^2 D + P_{j,i}^{(h)} \nabla_h^2 h + P_{j,i}^{(d)} \nabla_h^2 d \\ & + Q_{j,i}^{(D,D)} (\nabla_h D)^2 + Q_{j,i}^{(h,h)} (\nabla_h h)^2 + Q_{j,i}^{(d,d)} (\nabla_h d)^2 + \left(Q_{j,i}^{(d,h)} + Q_{j,i}^{(h,d)}\right)(\nabla_h d)\cdot(\nabla_h h) \\ & + \left(Q_{j,i}^{(D,h)} + Q_{j,i}^{(h,D)}\right)(\nabla_h D)\cdot(\nabla_h h) + \left(Q_{j,i}^{(D,d)} + Q_{j,i}^{(d,D)}\right)(\nabla_h D)\cdot(\nabla_h d). \end{aligned}$$

Explicit expressions for the inner-products that appear in the coefficients $b_{j,i}$, $\widetilde{\boldsymbol{d}}_{j,i}$ and $j_{j,i}$ are lengthy and may be found in the Appendix.

4.5. *The hybrid approximation*

As an alternative to the natural approximation, for use in situations in which bifurcations invalidate the use of the natural-evanescent modes, we introduce the *hybrid* MMA, defined as

$$\phi(x, y, z) \approx \hat{\psi}_N(x, y, z) = \hat{\varphi}_0(x, y)\cosh k_0(z + h) + \sum_{n=1}^{N} \hat{\varphi}_n(x, y)\cos l_n(z + h),$$

where $l_n = n\pi/H$ $(n = 1, \ldots)$.

Although, throughout §§5–6, it will be assumed that the MMA uses the natural modes, unless otherwise stated, algebraic manipulations hold for the hybrid modes; applications of the hybrid approximation are made in §7.

5. Two-dimensional problems and oblique incidence

We now consider the application of the MMA specifically to two-dimensional problems in which the bed-shape and ice-shape are independent of y; this is the situation shown in figure 1, now assumed to represent every cross-section. The geometry is permitted to vary over a finite interval with semi-infinite intervals of uniform geometry at both ends of this finite interval that are either ice-covered and run on continuously from the varying geometry (see figure 1) or are ice-free. Obliquely incident plane waves propagate from the far fields and have crests that meet the x-axis at a given angle. This situation has been considered by previous authors and comparative results are therefore available for some geometries.

This is an appropriate juncture at which to introduce the lateral conditions attached to the problem. For the two-dimensional problem described, the exact solution must satisfy the radiation conditions

$$\begin{aligned} \phi(x, y, z) \sim {} & \left\{A^{(\pm)} \exp\left(\pm \mathrm{i}\lambda_0^{(\pm)} x\right) + B^{(\pm)} \exp\left(\mp \mathrm{i}\lambda_0^{(\pm)} x\right)\right\} \\ & \times \exp(\mathrm{i}my)\cosh k_0^{(\pm)}\left(z + h^{(\pm)}\right) \quad (x \to \pm\infty), \end{aligned} \tag{5.1}$$

in which $k_0^{(\pm)}$ are the incident wavenumbers, $m = k_0^{(\pm)} \sin\theta^{(\pm)}$, where $\theta^{(\pm)}$ are the angles made by the incident waves with the x-axis, $(\lambda_0^{(\pm)})^2 = (k_0^{(\pm)})^2 - m^2$, $A^{(\pm)}$ are prescribed incoming amplitudes and $B^{(\pm)}$ are unknown outgoing amplitudes that must be determined as part of the solution process.

As a periodic variation has been assumed, it is pertinent to retain this in our approximation by setting:

$$\varphi_i(x, y) = \tilde{\varphi}_i(x)\mathrm{e}^{\mathrm{i}my} \quad (i = 0, \ldots, N); \quad \chi(x, y) = \tilde{\chi}(x)\mathrm{e}^{\mathrm{i}my}.$$

The unknown functions are relabelled $\tilde{\varphi}(x) \equiv \varphi(x)$ and $\tilde{\chi}(x) \equiv \chi(x)$. They, along with the functions that define the surrounding ice and bed shape, are now functions of the variable x only, and $w_i = w_i(x, z)$.

It is then straightforward to reduce the partial differential system (3.4) to

$$\partial_x(\boldsymbol{A}\partial_x\boldsymbol{\Phi}_N) + \widetilde{\boldsymbol{D}}\partial_x\boldsymbol{\Phi}_N + (\boldsymbol{B} - m^2\boldsymbol{A})\boldsymbol{\Phi}_N + \kappa\chi\boldsymbol{C}\boldsymbol{f} = \boldsymbol{0}, \tag{5.2}$$

and (3.2) to

$$\left\{\left(\partial_x^2 - m^2\right)\beta\left(\partial_x^2 - m^2\right) + (1-\nu)\left(\partial_x^2\beta\right)m^2 + 1 - \alpha\right\}\chi - \sum_{i=0}^{N}[w_i]_{z=-d}\varphi_i = 0, \tag{5.3}$$

where all of the matrices are defined in § 3. From here on, the notation ∂_x represents the full derivative $\mathrm{d}/\mathrm{d}x$. The following, more compact, version of this system of differential equations

$$\partial_x(\mathscr{A}\partial_x\boldsymbol{\Psi}_N) + \widetilde{\mathscr{D}}\partial_x\boldsymbol{\Psi}_N + \mathscr{B}\boldsymbol{\Psi}_N = \boldsymbol{0}, \tag{5.4}$$

will be used, where

$$\boldsymbol{\Psi}_N = \left(\boldsymbol{\Phi}_N^T, \chi^{(1)}, \chi^{(2)}\right)^T,$$

which is such that $\chi^{(1)} = \chi$, and $\chi^{(2)} = \beta(\partial_x^2 - m^2)\chi$, and

$$\begin{gathered}
\mathscr{A}_{i,j} = A_{i,j}, \quad \mathscr{B}_{i,j} = B_{i,j} - m^2A_{i,j}, \quad \widetilde{\mathscr{D}}_{i,j} = \widetilde{D}_{i,j} \quad (i, j = 1, \ldots, N+1), \\
\mathscr{A}_{N+2,N+2} = \mathscr{A}_{N+3,N+3} = 1, \quad \mathscr{B}_{i,N+2} = \kappa\boldsymbol{I}_i^T\boldsymbol{C}\boldsymbol{f} \quad (i = 1, \ldots, N+1), \\
\mathscr{B}_{N+2,N+3} = -\beta^{-1}, \quad \mathscr{B}_{N+3,j} = -\boldsymbol{f}^T\boldsymbol{C}\boldsymbol{I}_j \quad (j = 1, \ldots, N+1), \\
\mathscr{B}_{N+2,N+2} = \mathscr{B}_{N+3,N+3} = -m^2, \quad \mathscr{B}_{N+3,N+2} = (1-\nu)\left(\partial_x^2\beta\right)m^2 + 1 - \alpha,
\end{gathered}$$

with all unspecified values equal to zero and where $\boldsymbol{I} = [\boldsymbol{I}_1, \ldots, \boldsymbol{I}_{N+1}]$, is the identity matrix of size $N+1$.

The accompanying jump conditions must also be calculated. Given the restrictions of the problem, the contour Γ, over which the jump conditions are implemented, must be parallel to the y-axis and hence the normal to this contour is parallel to the x-axis. All conditions are assumed now to hold at the point $x = x_0$.

The two-dimensional versions of jump conditions (3.8), (3.9), (3.10) and (3.12) are

$$\langle\boldsymbol{\Phi}_N\rangle = \boldsymbol{0}, \quad \langle\boldsymbol{A}\partial_x\boldsymbol{\Phi}_N + \boldsymbol{J}\boldsymbol{\Phi}_N\rangle = \boldsymbol{0}, \tag{5.5}$$

and

$$\langle\overline{\boldsymbol{V}}^T\boldsymbol{\Phi}_N\rangle = \boldsymbol{0}, \quad \langle\boldsymbol{V}^{-1}\{\boldsymbol{A}\partial_x\boldsymbol{\Phi}_N + \boldsymbol{J}\boldsymbol{\Phi}_N\}\rangle = \boldsymbol{0}, \tag{5.6}$$

respectively, where $\boldsymbol{V}$ is defined in § 3.2.

The bending moment and shearing stress reduce to

$$\mathfrak{M}\chi = \hat{\chi}^{(2)} + \beta(1-\nu)m^2\hat{\chi}^{(1)}$$

and

$$\mathfrak{S}\chi = \partial_x\hat{\chi}^{(2)} - (1-\nu)m^2(\beta\partial_x - (\partial_x\beta))\hat{\chi}^{(1)}.$$

For continuous ice-cover, the essential conditions to be applied are $\langle\varphi_i\rangle = 0$ $(i = 0, \ldots, N)$ and $\langle\hat{\chi}^{(1)}\rangle = \langle\partial_x\hat{\chi}^{(1)}\rangle = 0$. The latter may be used to simplify the

conditions of continuity of bending moment and shearing stress to

$$\langle \hat{\chi}^{(2)} \rangle = 0,$$

and

$$\langle \partial_x \hat{\chi}^{(2)} + (1-\nu)m^2(\partial_x \beta)\hat{\chi}^{(1)} \rangle = 0,$$

respectively.

The full set of jump conditions at a point at which two intervals of connected ice meet may then be expressed as

$$\langle \boldsymbol{\Psi}_N \rangle = \mathbf{0}, \tag{5.7}$$

and

$$\langle \mathscr{A} \partial_x \boldsymbol{\Psi}_N + \mathscr{J} \boldsymbol{\Psi}_N \rangle = \mathbf{0}, \tag{5.8}$$

where $\mathscr{J}_{n,m} = J_{n,m}$ $(n, m = 1, \ldots, N+1)$ and $\mathscr{J}_{N+3,N+2} = (1-\nu)m^2(\partial_x \beta)$, with all unspecified entries being zero.

If, however, the jump conditions are to be applied at a point separating ice-covered and free-surface fluid intervals, then no essential conditions are applied, and the jump conditions are given by (5.6) as

$$\hat{\chi}_+^{(2)} + \beta_+(1-\nu)m^2 \hat{\chi}_+^{(1)} = 0 \tag{5.9}$$

and

$$\partial_x \hat{\chi}_+^{(2)} - (1-\nu)m^2(\beta_+ \partial_x - (\partial_x \beta_+))\hat{\chi}_+^{(1)} = 0. \tag{5.10}$$

5.1. *Uniform geometry*

In a situation in which the geometric variables D, h and d take constant values, it is possible to give an analytic expression for the natural MMA, as (5.4) reduces to a constant-coefficient ordinary differential system that may be solved by standard methods.

Therefore, take $\boldsymbol{\Psi}_N(x) = \hat{\boldsymbol{c}}(\lambda)\mathrm{e}^{\mathrm{i}\lambda x}$, such that $\hat{\boldsymbol{c}}^T(\lambda) = (\boldsymbol{c}^T(\lambda), \gamma^{(1)}(\lambda), \gamma^{(2)}(\lambda))$, where λ is a constant and $\hat{\boldsymbol{c}}(\lambda)$ is a constant vector, representing eigenvalues and eigenvectors of the system, respectively. Substituting these expressions into (5.2) and (5.3), and making use of

$$\widetilde{d}_{j,i} = 0, \quad b_{j,i} = a_{j,i}k_i^2 - k_i \sinh(k_i H)\cosh(k_j H),$$

which apply on intervals of constant D, h and d, leaves the eigensystem defined by

$$(\boldsymbol{A}(\boldsymbol{K}^2 - (\lambda^2 + m^2)\boldsymbol{I}) - \boldsymbol{C}\boldsymbol{f}\boldsymbol{f}^T\boldsymbol{K}\boldsymbol{S})\boldsymbol{c} + \kappa\gamma^{(1)}\boldsymbol{C}\boldsymbol{f} = \mathbf{0}, \tag{5.11}$$

and

$$(\beta(\lambda^2 + m^2)^2 + 1 - \alpha)\gamma^{(1)} - \boldsymbol{f}^T\boldsymbol{C}\boldsymbol{c} = 0, \tag{5.12}$$

where $\boldsymbol{C} = \mathrm{diag}\{\cosh(k_0 H), \ldots, \cosh(k_N H)\}$, $\boldsymbol{S} = \mathrm{diag}\{\sinh(k_0 H), \ldots, \sinh(k_N H)\}$ and $\boldsymbol{K} = \mathrm{diag}\{k_0, \ldots, k_N\}$, which is to be solved for eigenvalues λ and corresponding eigenvector entries $\boldsymbol{c}(\lambda)$ and $\gamma^{(1)}(\lambda)$. (The constant $\gamma^{(2)}(\lambda)$ is not required; its value is easily recovered from $\gamma^{(1)}(\lambda)$.)

Manipulations, using (4.6) and (5.12), reduce (5.11) to

$$(\boldsymbol{K}^2 - (\lambda^2 + m^2)\boldsymbol{I})\boldsymbol{A}\boldsymbol{c} + \beta\gamma^{(1)}(\boldsymbol{K}^2 - (\lambda^2 + m^2)\boldsymbol{I})(\boldsymbol{K}^2 + (\lambda^2 + m^2)\boldsymbol{I})\boldsymbol{K}\boldsymbol{S}\boldsymbol{f} = \mathbf{0}. \tag{5.13}$$

At this point, it may be noted that the $2N+2$ pairs

$$(\lambda^2, \boldsymbol{c}) = \left(\lambda_i^2, \boldsymbol{I}_{i+1}\right) \equiv \left(k_i^2 - m^2, \boldsymbol{I}_{i+1}\right) \quad (i = 0, \ldots, N),$$

satisfy (5.13), and hence provide our first set of eigenvalue–eigenvector pairs. The values $\gamma^{(1)}(\lambda_i) = \kappa^{-1} k_i \sinh(k_i H)$ $(i = 0, \ldots, N)$, may be recovered from (5.12). To find the remaining four eigenvector–eigenvalue pairs, we return to (5.13) and note that for $\lambda \neq \lambda_i$ $(i = 0, \ldots, N)$, the matrix $\boldsymbol{K}^2 - (\lambda^2 + m^2)\boldsymbol{I}$ is non-singular, and hence

$$\boldsymbol{A}\boldsymbol{c} + \beta\gamma^{(1)}(\boldsymbol{K}^2 + (\lambda^2 + m^2)\boldsymbol{I})\boldsymbol{K}\boldsymbol{S}\boldsymbol{f} = \boldsymbol{0}, \tag{5.14}$$

and (using (5.12))

$$(\beta(\lambda^2 + m^2)^2 + 1 - \alpha) + \beta \boldsymbol{f}^T \boldsymbol{C}\boldsymbol{A}^{-1}(\boldsymbol{K}^2 + (\lambda^2 + m^2)\boldsymbol{I})\boldsymbol{K}\boldsymbol{S}\boldsymbol{f} = 0. \tag{5.15}$$

Equation (5.15) is a quartic which defines the remaining four eigenvalues

$$\lambda^2 = \lambda_{-i}^2 \equiv \mu_{N,(i)}^2 - m^2 \quad (i = 1, 2).$$

The corresponding eigenvectors are then recovered from (5.14). Note that the choice of $\gamma^{(1)}(\lambda_{-i})$ $(i = 1, 2)$ is free, and will be set as 1 for simplicity.

For the vertical modes used in the approximation, the eigenvalue–eigenvector pairs $(\lambda_i, \boldsymbol{I}_i)$ $(i = 0, \ldots, N)$ provide the horizontal waves attached to each of the modes in the full linear solution of the uniform problem, when all of the vertical modes are included. The role played by the eigenvalue–eigenvector pairs $(\lambda_{-i}, \boldsymbol{c}(\lambda_{-i}))$ $(i = 1, 2)$ mirrors that of the waves belonging to the vertical modes that are removed from the vertical expansion of the full linear solution, which become redistributed amongst the remaining vertical modes. As we have truncated the vertical motion to a finite dimension, these eigenvalue–eigenvector pairs attempt to compensate for all of the modes missing from the approximation and are sensitive to the addition of further modes to the approximation. In the limit $N \to \infty$, the eigenvalues will converge to the exact horizontal waves of the omitted vertical modes and the eigenvectors to the weightings that they are given on redistribution to the remaining modes.

On intervals of constant D, h and d the approximation may therefore be written as

$$\boldsymbol{\Psi}_N(x) = \mathscr{C}\{\exp(\mathrm{i}\boldsymbol{\Lambda}x)\boldsymbol{A} + \exp(-\mathrm{i}\boldsymbol{\Lambda}x)\boldsymbol{B}\},$$

where

$$\boldsymbol{\Lambda} = \mathrm{diag}\{\lambda_0, \ldots, \lambda_N, \lambda_{-1}, \lambda_{-2}\}, \quad \exp(\pm\mathrm{i}\boldsymbol{\Lambda}x) = \mathrm{diag}\{\exp(\pm\mathrm{i}\lambda_0 x), \ldots, \exp(\pm\mathrm{i}\lambda_N x), \exp(\pm\mathrm{i}\lambda_{-1}x), \exp(\pm\mathrm{i}\lambda_{-2}x)\},$$

$$\mathscr{C} = [\hat{\boldsymbol{c}}(\lambda_0), \cdots \hat{\boldsymbol{c}}(\lambda_N),\ \hat{\boldsymbol{c}}(\lambda_{-1}),\ \hat{\boldsymbol{c}}(\lambda_{-2})],$$

and $\boldsymbol{A}$ and $\boldsymbol{B}$ are constant vectors of length $N + 3$. In an interval of free-surface fluid, the above expression degenerates to

$$\boldsymbol{\Phi}_N(x) = \exp(\mathrm{i}\boldsymbol{\Lambda}x)\boldsymbol{A} + \exp(-\mathrm{i}\boldsymbol{\Lambda}x)\boldsymbol{B},$$

in which $\boldsymbol{\Lambda} = \mathrm{diag}\{\lambda_0, \ldots, \lambda_n\}$, where $\lambda_i^2 = (k_i^{(0)})^2 - m^2$ $(i = 0, \ldots, N)$, and $\boldsymbol{A}$ and $\boldsymbol{B}$ are now of length $N + 1$. We note that a benefit of the natural approximation is that the exact radiation conditions, equation (5.1), are retained.

In this section we have ignored the possibility of the approximate roots $\mu_{N,(i)}$ $(i = 1, 2)$ coinciding, which could occur even though a double root of the dispersion relation is not present. This situation is easily dealt with by standard methods. It is also noted that, in the neighbourhood of a true bifurcation, it is not unlikely that the properties of the $\mu_{N,(i)}$ $(i = 1, 2)$ differ from those of the μ_i $(i = 1, 2)$. That is, for certain N, the $\mu_{N,(i)}$ $(i = 1, 2)$ may be purely imaginary, whilst the μ_i $(i = 1, 2)$ are complex and vice versa.

6. Numerical formulation

Two specific versions of the two-dimensional problem will be considered. In both, fluid occupies the domain $(x, z) \in (-\infty, \infty) \times (-h, -d)$, with the fluid and ice boundaries only varying over the finite interval $x \in (0, l)$, and uniform states in the semi-infinite intervals to either side.

The following account assumes the use of natural modes throughout $-\infty < x < \infty$; however, if bifurcations occur and prevent this approach then we revert to the hybrid modes (see §4.5) in the interval $x \in (0, l)$ making the appropriate adjustments to the following formulation.

6.1. *Continuous ice-cover*

For the first problem, it is assumed that $D(x) \neq 0$ for all x and that all geometrical variables are continuous functions of x and we apply the natural approximation throughout the fluid region.

In the two semi-infinite intervals of constant ice thickness and fluid depth, the approximation is given by

$$\boldsymbol{\Psi}_N^{(-)}(x) = \boldsymbol{\mathscr{C}}^{(-)}\left\{\exp\left(\mathrm{i}\boldsymbol{\Lambda}^{(-)}x\right)\boldsymbol{A}^{(-)} + \exp\left(-\mathrm{i}\boldsymbol{\Lambda}^{(-)}x\right)\boldsymbol{B}^{(-)}\right\} \quad (x < 0), \tag{6.1a}$$

$$\boldsymbol{\Psi}_N^{(+)}(x) = \boldsymbol{\mathscr{C}}^{(+)}\left\{\exp\left(\mathrm{i}\boldsymbol{\Lambda}^{(+)}(l-x)\right)\boldsymbol{A}^{(+)} + \exp\left(-\mathrm{i}\boldsymbol{\Lambda}^{(+)}(l-x)\right)\boldsymbol{B}^{(+)}\right\} \quad (x > l), \tag{6.1b}$$

where vectors $\boldsymbol{A}^{(\pm)} = (A_0^{(\pm)}, 0, \ldots, 0, 0, 0)^T$ contain the known incoming amplitudes and $\boldsymbol{B}^{(\pm)} = (B_{N,0}^{(\pm)}, \ldots, B_{N,N}^{(\pm)}, B_{N,-1}^{(\pm)}, B_{N,-2}^{(\pm)})^T$ contain unknown outgoing amplitudes. The superscripts $^{(\pm)}$ are used to denote that the function belongs to the corresponding interval of uniform geometry. The approximation therefore mirrors the exact radiation conditions (5.1), so that in the far fields

$$\psi_N \sim \begin{cases} \left\{A_0^{(-)}\exp\left(\mathrm{i}\lambda_0^{(-)}x\right) \right. \\ \quad \left. + B_{N,0}^{(-)}\exp\left(-\mathrm{i}\lambda_0^{(-)}x\right)\right\}\exp(\mathrm{i}my)\cosh\left\{k_0^{(-)}\left(z+h^{(-)}\right)\right\} & (x \to -\infty), \\ \left\{A_0^{(+)}\exp\left(\mathrm{i}\lambda_0^{(+)}(l-x)\right)\right. \\ \quad \left. + B_{N,0}^{(+)}\exp\left(-\mathrm{i}\lambda_0^{(+)}(l-x)\right)\right\}\exp(\mathrm{i}my)\cosh\left\{k_0^{(+)}\left(z+h^{(+)}\right)\right\} & (x \to \infty), \end{cases}$$

and thus the only approximation is to the outgoing amplitudes $B_{N,0}^{(\pm)}$.

It is computationally efficient to suppress as many unknowns as possible. With this in mind, the jump conditions (5.7)–(5.8), applied at $x = 0, l$ with (6.1*a*,*b*) used in the intervals of uniform geometry, are reformulated as

$$\mathfrak{B}_\pm \boldsymbol{\Psi}_N(x^{(\pm)}) = \mp\mathrm{i}\lambda_0\left(A_0^{(\pm)} - B_{N,0}^{(\pm)}\right)\boldsymbol{\mathscr{A}}^{(\pm)}\boldsymbol{\mathscr{C}}^{(\pm)}\boldsymbol{\mathscr{I}}_1$$

where $\boldsymbol{\mathscr{I}}_1 = (1, 0 \ldots, 0)^T$ is of length $N+3$, and

$$\mathfrak{b}_\pm \boldsymbol{\Psi}_N\left(x^{(\pm)}\right) = A_0^{(\pm)} + B_{N,0}^{(\pm)}, \tag{6.2}$$

where $x^{(\pm)} = (l \pm l)/2$,

$$\mathfrak{B}_\pm \boldsymbol{v}(x) \equiv (\boldsymbol{\mathscr{A}}(x_\mp)\partial_x + \widetilde{\boldsymbol{\mathscr{J}}}_\pm(x))\boldsymbol{v}(x_\mp),$$

and

$$\mathfrak{b}_\pm \boldsymbol{v}(x) \equiv \boldsymbol{\mathscr{I}}_1^T \boldsymbol{\mathscr{C}}^{-1}(x_\pm)\boldsymbol{v}(x_\mp),$$

where

$$\widetilde{\boldsymbol{\mathscr{J}}}_\pm(x) = \boldsymbol{\mathscr{J}}(x_\mp) \mp \mathrm{i}\boldsymbol{\mathscr{A}}(x_\pm)\boldsymbol{\mathscr{C}}(x_\pm)\boldsymbol{\Lambda}(x_\pm)\widetilde{\boldsymbol{\mathscr{J}}}\boldsymbol{\mathscr{C}}^{-1}(x_\pm),$$

with $\widetilde{\mathscr{I}} = \mathrm{diag}\{0, 1, \ldots, 1\}$. Note that the only unknown amplitudes appearing in these new conditions are those of the outgoing amplitudes that appear in the far field, namely $B^{\pm}_{N,0}$.

The approximation is expressed over the interval $x \in (0, l)$ as a linear combination of numerically determinable functions

$$\boldsymbol{\Psi}_N(x) = \mathrm{i}\big(A_0^{(-)} - B_{N,0}^{(-)}\big)\mathscr{L}_-(x) + \mathrm{i}\big(A_0^{(+)} - B_{N,0}^{(+)}\big)\mathscr{L}_+(x),$$

where $\mathscr{L}_\pm$ satisfy (5.4), with

$$\mathfrak{B}_-\mathscr{L}_-(0) = \lambda_0^{(-)}\mathscr{A}^{(-)}\mathscr{C}^{(-)}\mathscr{I}_1, \quad \mathfrak{B}_+\mathscr{L}_+(l) = -\lambda_0^{(+)}\mathscr{A}^{(+)}\mathscr{C}^{(+)}\mathscr{I}_1,$$

and

$$\mathfrak{B}_+\mathscr{L}_-(l) = \mathfrak{B}_-\mathscr{L}_+(0) = \mathbf{0}.$$

Application of the remaining conditions (6.2) leads to

$$\begin{pmatrix} B_{N,0}^{(-)} \\ B_{N,0}^{(+)} \end{pmatrix} = \boldsymbol{S} \begin{pmatrix} A_0^{(-)} \\ A_0^{(+)} \end{pmatrix}, \tag{6.3}$$

where the scattering matrix is

$$\boldsymbol{S} = -(\boldsymbol{I}_2 + \mathrm{i}\boldsymbol{P})^{-1}(\boldsymbol{I}_2 - \mathrm{i}\boldsymbol{P}),$$

with $\boldsymbol{I}_2$ representing the two-dimensional identity matrix, and

$$\boldsymbol{P} = \begin{pmatrix} \mathfrak{b}_-\mathscr{L}_-(0) & \mathfrak{b}_-\mathscr{L}_+(0) \\ \mathfrak{b}_+\mathscr{L}_-(l) & \mathfrak{b}_+\mathscr{L}_+(l) \end{pmatrix}. \tag{6.4}$$

The unknown outgoing amplitudes $B_{N,0}^{(\pm)}$ are thereby determined directly.

6.2. *Partial ice-cover*

In the second situation considered, the ice-cover is restricted to the finite interval $x \in (0, l)$. This interval also represents the only interval in which the bed geometry is permitted to vary. The constant intervals to either side are occupied by free surface fluid ($D = 0$).

The analytic expressions for the MMA in the free-surface intervals are

$$\boldsymbol{\Phi}_N^{(-)}(x) = \exp\big(\mathrm{i}\boldsymbol{\Lambda}^{(-)}x\big)\boldsymbol{A}^{(-)} + \exp\big(-\mathrm{i}\boldsymbol{\Lambda}^{(-)}x\big)\boldsymbol{B}^{(-)} \qquad (x < 0),$$
$$\boldsymbol{\Phi}_N^{(+)}(x) = \exp\big(\mathrm{i}\boldsymbol{\Lambda}^{(+)}(l-x)\big)\boldsymbol{A}^{(+)} + \exp\big(-\mathrm{i}\boldsymbol{\Lambda}^{(+)}(l-x)\big)\boldsymbol{B}^{(+)} \quad (x > l),$$

with all arrays having degenerated to their free-surface equivalent (see § 5.1). The radiation conditions again dictate that the only non-zero incoming amplitudes are $A_0^{(\pm)}$, belonging to the propagating waves.

The reformulated versions of (5.6) and (5.9)–(5.10), applied at $x = 0, l$ are

$$\mathfrak{B}_\pm\boldsymbol{\Psi}_N\big(x^{(\pm)}\big) = \mp\mathrm{i}\lambda_0^{(\pm)}\big(A_0^{(\pm)} - B_{N,0}^{(\pm)}\big)\big(\mathscr{V}^{(\pm)}\big)^{-1}\mathscr{A}^{(\pm)}\mathscr{I}_1$$

and

$$\mathfrak{b}_\pm\boldsymbol{\Phi}_N(x^{(\pm)}) = A_0^{(\pm)} + B_{N,0}^{(\pm)},$$

where we have redefined $\mathfrak{B}_\pm$ and $\mathfrak{b}_\pm$ as

$$\mathfrak{B}_\pm\boldsymbol{v}(x) \equiv (\hat{\mathscr{A}}(x_\mp)\partial_x + \widetilde{\mathscr{J}}_\pm(x))\boldsymbol{v}(x_\mp)$$

and

$$\mathfrak{b}_\pm\boldsymbol{v}(x) \equiv \boldsymbol{I}_1^T\boldsymbol{V}^{-T}(x_\pm)\mathscr{V}^T(x_\mp)\boldsymbol{v}(x_\mp).$$

Where

$$(\hat{\mathscr{A}}(x))_{j,i} = (V^{-1}(x)A(x))_{j,i} \quad (i,\, j = 1, \ldots, N+1), \quad (\hat{\mathscr{A}}(x))_{N+3,N+2} = -\beta(x)(1-\nu)m^2,$$

$\hat{\mathscr{A}}_{N+3,N+3} = 1$ and $\mathscr{J}_{\pm}$ is now defined by

$$(\widetilde{\mathscr{J}}_{\pm}(x))_{n,m} = (\boldsymbol{V}^{-1}(x_{\mp})\boldsymbol{J}(x_{\mp}) \mp \mathrm{i}V^{-1}(x_{\pm})\boldsymbol{A}(x_{\pm})\boldsymbol{\Lambda}(x_{\pm})\widetilde{\boldsymbol{I}}\boldsymbol{V}^{-T}(x_{\pm})\boldsymbol{V}^{T}(x_{\mp}))_{n,m},$$

with $\widetilde{\boldsymbol{I}} = \mathrm{diag}\{0, 1, \ldots, 1\}$, for $n, m = 1, \ldots, N+1$ and

$$\widetilde{\mathscr{J}}_{\pm}(x)_{N+2,N+3} = 1, \quad (\widetilde{\mathscr{J}}_{\pm}(x))_{N+2,N+2} = (1-\nu)m^2\beta(x_{\mp}),$$
$$(\widetilde{\mathscr{J}}_{\pm}(x))_{N+3,N+2} = (1-\nu)m^2\partial_x\beta(x_{\mp}).$$

Again, all unspecified entries are zero.

Solving using linearity, we have

$$\boldsymbol{\Psi}_N(x) = \mathrm{i}\big(A_0^{(-)} - B_{N,0}^{(-)}\big)\mathscr{L}_-(x) + \mathrm{i}\big(A_0^{(+)} + B_{N,0}^{(+)}\big)\mathscr{L}_+(x),$$

for $0 < x < l$, where the numerically determined functions $\mathscr{L}_{\pm}$ satisfy (5.4), and the boundary conditions

$$\mathfrak{B}_-\mathscr{L}_-(0) = \lambda_0^{(-)}\mathscr{V}^{-1}(0_-)\mathscr{A}(0_-)\mathscr{I}_1,$$
$$\mathfrak{B}_+\mathscr{L}_+(l) = -\lambda_0^{(+)}\mathscr{V}^{-1}(l_+)\mathscr{A}(l_+)\mathscr{I}_1,$$

and

$$\mathfrak{B}_-\mathscr{L}_+(0) = \mathfrak{B}_+\mathscr{L}_-(l) = \mathbf{0}.$$

The unknown outgoing amplitudes $B_{N,0}^{(\pm)}$ are again determined using (6.3)–(6.4).

7. Results

Results presented in this section have been calculated using a central finite-difference numerical solver for the ODEs that arise in the intervals of varying geometry. This simple method is sufficient for the problems considered here although it can be expected that difficulties would be experienced for problems in which rapidly decaying/growing modes are present. This may be caused by a particularly small value of D, for which μ becomes large, or a large value of N as $k_N = O(N)$. When intervals of uniform geometry are present in $x \in (0, l)$, the analytic form of the natural approximation may act as a check on the numerical solver.

To confirm the validity of the MMA as well as examine its convergence properties, it is pertinent to compare solutions obtained by the present method with those of previous authors, before producing new results using geometrical configurations that fully exploit the MMA. For the purposes of this paper, the results will be considered to have converged when consecutive computational approximations, of dimensions N and $N+1$, have a relative difference, $\epsilon_N < 5 \times 10^{-2}$, although it must be noted that this is an arbitrary choice.

Belibassakis & Athanassoulis (2005) used a variational approach to solve the two-dimensional problem for an ice sheet of constant thickness and with zero draught. Noting that the natural modes satisfy $[\partial_z w_i]_{z=-h} = 0$ and building on their earlier work for free-surface motions (Belibassakis & Athanassoulis 1999), they included an extra expansion mode, $\tilde{\tilde{w}}$ say, satisfying $[\partial_z \tilde{\tilde{w}}]_{z=-h} \neq 0$, and thereby accelerated the convergence of the approximation.

In the particular problem chosen for comparison, $\alpha = 0$, $\beta = 10^5\,\mathrm{Pa\,m^5\,s^2\,kg^{-1}}$ and $l = 500\,\mathrm{m}$, with

$$h(x) = \frac{h_0 + h_1}{2} - \frac{h_0 - h_1}{2}\tanh 3\pi(x/l - 1/2) \quad (0 < x < l). \tag{7.1}$$

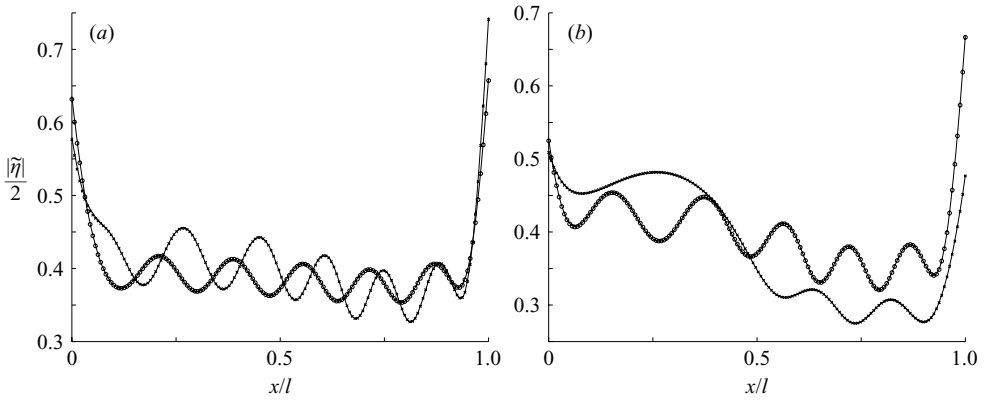

FIGURE 2. Comparison with figures 10–11 of Belibassakis & Athanassoulis (2005). Partial ice-cover; bed shape (7.1) and floe length $l = 500\,\mathrm{m}$. Symbols are single-mode approximations ($N = 0$) and solid lines are two-mode approximations ($N = 1$). (*a*) $\theta = 0$: ○, $h_0 = 12\,\mathrm{m}$, $h_1 = 8\,\mathrm{m}$; ×, $h_0 = 15\,\mathrm{m}$, $h_1 = 5\,\mathrm{m}$, (*b*) $h_0 = 15\,\mathrm{m}$, $h_1 = 5\,\mathrm{m}$: ○, $\theta = \pi/6$, × $\theta = \pi/3$.

Using the parameter values given in § 2, $\beta = 10^5\,\mathrm{Pa\,m^5\,s^2\,kg^{-1}}$ corresponds to an ice thickness $D_0 \approx 1.3\,\mathrm{m}$; however, although, from an algebraic point of view, the present theory admits the value $\alpha = 0$, this has no physical interpretation in our model. Figures 2(*a*) and 2(*b*) are the counterparts of figures 10 and 11 of Belibassakis & Athanassoulis (2005). Both figures plot the convergence of natural approximations to the magnitude of non-dimensionalized sheet elevation $|\widetilde{\eta}| = \mathrm{sech}(k_0 H)^{(-)}|\eta|/A_0^{(-)}$ across the ice floe; the single incoming wave has angular frequency $\omega = 0.4\,\mathrm{rad\,s^{-1}}$. Only the most significant two sets of data are plotted on each graph to keep them uncluttered. The four parameter sets each demonstrate extremely rapid convergence with $\epsilon_0 \approx 1 \times 10^{-3}$ in all cases. The converged curves of figure 2 appear identical to their counterparts in Belibassakis & Athanassoulis (2005).

A restricted case of varying ice thickness in two-dimensions was solved by Williams & Squire (2004), who considered variations in the upper surface of the ice (sail heterogeneities) in infinite intervals of complete ice-cover. Their method of solution used a Green's function that allowed the vertical displacement of the underside of the ice to be obtained from an integral equation, which leads to a knowledge of the reduced velocity potential everywhere.

Here, two examples of sail heterogeneities used by Williams & Squire have been chosen to provide comparison with the MMA. The first, described as *type 1* by Williams & Squire, is defined by

$$D(x) = \begin{cases} 1 & (x < 0), \\ 1 + 2x/15 & (0 < x < 15/2), \\ 3 - 2x/15 & (15/2 < x < 15), \\ 1 & (x > 15). \end{cases}$$

The second, described as *type 2* by Williams & Squire, is defined by

$$D(x) = \begin{cases} 1 & (x < 0), \\ 2 & (0 < x < 15), \\ 1 & (x > 15). \end{cases}$$

In both problems, $d = 0$ and $h = 70\,\mathrm{m}$. For the type 2 sail, we encounter the problem of discontinuities in the ice thickness. As indicated in § 2.4.2, the ability to use a consistent

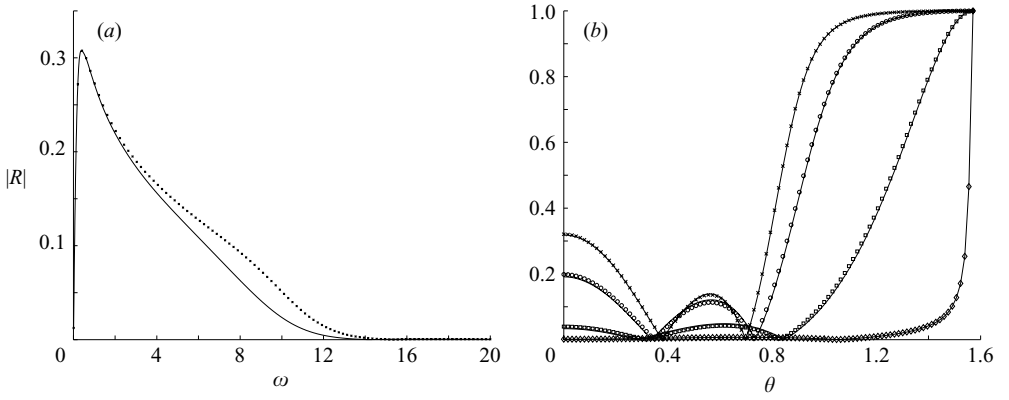

FIGURE 3. Comparison with figures 4(*e*) and 4(*i*) of Williams & Squire (2004). Complete ice-cover: (*a*) sail of type 1; (*b*) sail of type 2. Symbols are single-mode approximations ($N=0$), solid lines are converged approximations ((*a*) $N=2$, (*b*) $N=1$). (*a*) $\theta=0$; (*b*) $\times$, ($\omega=\pi\,\mathrm{rad\,s^{-1}}$); $\circ$, ($\omega=2\pi/5\,\mathrm{rad\,s^{-1}}$); $\square$, ($\omega=\pi/5\,\mathrm{rad\,s^{-1}}$); $\diamond$, ($\omega=2\pi/15\,\mathrm{rad\,s^{-1}}$).

MMA rests on the removal of the essential condition $\langle\langle\psi_N\rangle\rangle=0$, and insertion of the functional I_Γ, which, as the fluid depth is continuous, requires no modification. This effectively replaces (5.5) with (5.6), with (5.7)–(5.8) amended accordingly.

Figures 3(*a*) and 3(*b*) are for comparison to figures 4(*e*) and 4(*i*) of Williams & Squire (2004). Both plot converged natural approximations to the magnitude of the reflected amplitude against incoming wave period (figure 3*a*) or incident angle (figure 3*b*), along with the corresponding single-mode approximations. The graphs of the transmitted amplitudes have been omitted for clarity. Again the converged curves compare well with the original curves of Williams & Squire (2004). In figure 3(*a*), three natural modes are required for convergence. The single-mode approximation and fully converged approximation have a relative difference of approximately 1.2×10^{-1}, that is produced mainly by quantitative inaccuracies that occur in the middle of the wide interval of incoming wave periods. For figure 3(*b*), the single-mode approximations provide suitably accurate approximations, with the double-mode approximations virtually overlapping them. Furthermore, the shift between the single- and double-mode approximations appear insensitive to the angle of incidence. There is no evidence in figure 3(*b*) that the jump in the trial functions produced by the discontinuity in the ice thickness D has caused the approximation any difficulties.

For the remainder of the results, we turn to geometrical configurations that are unsolvable by existing, alternative methods. Specifically, we are now at liberty to allow for variations in d, which includes the possibility of a non-zero draught. We begin with cases of continuous ice-cover. From here on, only normally incident waves ($\theta=0$) are taken.

The problems considered by PP for cases of complete ice-cover do not provide an adequate test of the MMA as they were restricted by the need for slowly varying geometry. For example, in the problems considered for figure 2(*a*) of PP, increments to the dimension of the approximation make at most $O(10^{-2})$ differences. Moreover, the PP results for geometrical configurations involving variations in d are complicated by the issue of missing terms discussed at the end of § 3. The results shown in figure 4(*a*) involve keels defined by $D(x)=D_0+d(x)$ and $d(x)=u(x)$, where

$$u(x)=\begin{cases}0 & (x<0,\ x>l),\\ A_u(1-\cos(2\pi x/l))/2 & (0<x<l),\end{cases}\tag{7.2}$$

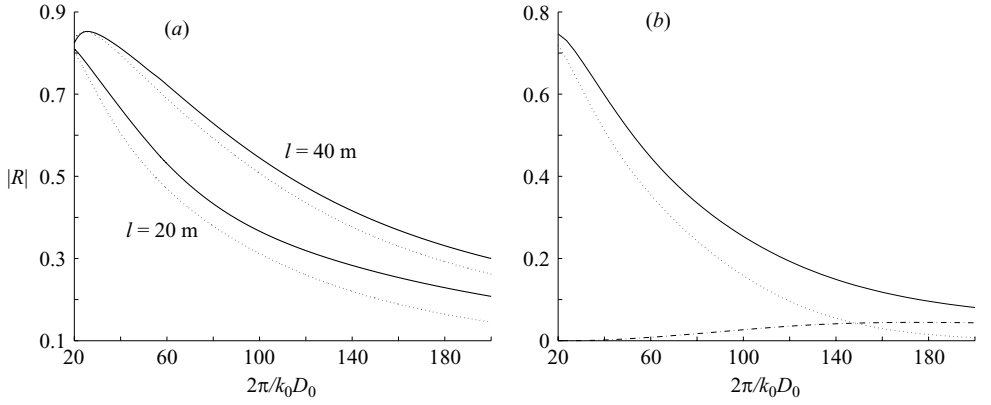

FIGURE 4. Continuous ice-cover: $D_0 = 1$ m, $h_0 = 20$ m. (*a*) $D(x) = D_0 + u(x)$ and $d(x) = u(x)$: $A_u = 10$ m. Dotted lines are single-mode approximations ($N = 0$), solid lines are converged hybrid approximations ($N = 4$ for $l = 20$ m, $N = 3$ for $l = 40$ m); (*b*) Converged hybrid approximations. Amplitude $A_u = 5$ m and length $l = 20$ m. $D(x) = D_0 + u(x)$ and $d(x) = u(x)$, $N = 2$ (solid); $D(x) = D_0 + u(x)$ and $d(x) = 0$, $N = 2$ (dotted); $h(x) = h_0 - u(x)$, $N = 1$ (dot-dash).

which are generalized versions of the geometry used by PP for their figure 2(*a*). Here, the – clearly non-slowly varying – amplitude $A_u = 10$ m is used and a constant bed depth, $h = 20$ m, is taken. For the interval of incoming wavelengths $2\pi/k_0 D_0 \in (20, 200)$, the natural-evanescent modes are unavailable for all values less than $2\pi/k_0 D_0 \approx 56.7$ owing to bifurcations on the first purely imaginary branch. We take this opportunity to use the hybrid approximation that was introduced in § 4.5. Figure 4(*a*) displays converged hybrid approximations for the problem described using the keel lengths $l = 20$ m and $l = 40$ m alongside the corresponding single-mode approximations. It can be seen here that, even for these rapidly varying keels, a single mode provides a good approximation; in both cases shown, it manages to represent accurately the shape and magnitude of the full linear solution. The convergence of the approximation to the smoother impediment, the 40 m keel, is more rapid than that of the 20 m keel, with $\epsilon_n = O(10^{-4})$ for $n = 3$ when $l = 40$ m compared to $n = 4$ for $l = 40$ m. Moreover, the single-mode approximation for the 40 m keel is more accurate than its counterpart for the 20 m keel by an order of magnitude. In the interval $2\pi/k_0 D_0 \in (56.7, 200)$ the natural approximations are at most of $O(10^{-4})$ different from their hybrid counterparts and for this reason it is not necessary to include this data in the figure.

In figure 4(*b*), we investigate the effect that the positions of an impediment has on the amount of energy it reflects, in the context of continuous ice-cover. The three curves displayed represent converged hybrid approximations to $|R|$ for a sail, a keel and a protrusion on the bed, all of the shape $u(x)$ such that $A_u = 5$ m. It is evident that the bed protrusion reflects significantly less energy than the equivalent variations to the thickness of the ice, for all the short- and mid-range wavelengths shown. A further phenomenon is that the sail and keel problems produce similar results, especially for shorter wavelengths. This similarity supports a conjecture made in Vaughan & Squire (2007). Across the range of incoming wavelenths, the keel reflects a greater amount of energy than the sail. Extensive numerical tests have shown the behaviour exhibited in figure 4(*b*) to be true generally.

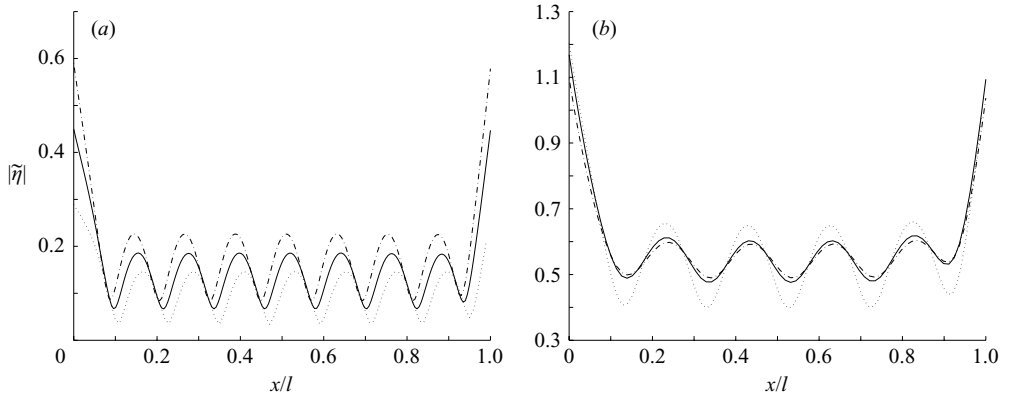

FIGURE 5. Comparison with figures 8(*a*) and 9(*a*) of PP. Partial ice-cover; $D_0 = 38$ mm, $l = 10$ m, $H_0 = 1.1$ m. Dotted line (PP single-mode approximation), dot-dash line (single-mode approximation, $N = 0$), solid line (converged MMA: (*a*) $N = 3$; (*b*) $N = 2$). (*a*) $\omega = 2\pi/0.7\,\mathrm{rad\,s^{-1}}$; (*b*) $\omega = 2\pi/1.429\,\mathrm{rad\,s^{-1}}$.

The results are concluded with cases of partial ice-cover. In all of the partial ice-cover situations we present in this paper, the parameter ranges are such that no bifurcations occur and the natural modes may be used.

In figure 5, the effect of the reformulation of the matching conditions given in PP are investigated. The figures display convergence of the natural approximation to the non-dimensional sheet elevation, $|\widetilde{\eta}|$, of a uniform floe of zero draught, length $l = 10$ m and thickness 38 mm over a uniform bed of depth 1.1m for two incoming wavelengths. The corresponding single-mode approximations of PP (originally appearing in figures 8*a* and 9*a* of PP) are also shown. For the incoming wave of angular frequency $\omega = 2\pi/0.7\,\mathrm{rad\,s^{-1}}$ (figure 5*a*), there is negligible difference between the accuracies of the single-mode approximations; however, for the incoming wave of angular frequency $\omega = 2\pi/1.429\,\mathrm{rad\,s^{-1}}$ (figure 5*b*), the reformulated matching conditions lead to a clear improvement in accuracy. The convergence of the natural approximation for the longer incoming wave is far more rapid than that of the shorter incoming wave, with $\epsilon_1 \approx 7.2 \times 10^{-3}$ for the longer wave compared to $\epsilon_2 \approx 3.7 \times 10^{-2}$ for the shorter wave. Furthermore, the single-mode approximation for the longer wave is an order of magnitude more accurate than that corresponding to the shorter wave.

It was anticipated in PP that a single-mode approximation may struggle to represent accurately the scattering process that occurs at the edges of an ice floe in a partial ice-cover setting. This hypothesis is examined in figure 6(*a*) using a uniform floe of zero draught, length 10 m and thickness 1 m over a uniform bed depth of 20 m. Here, three curves display the convergence of the natural approximation to the reflected energy, $|R|$, for this problem, over a range of incoming wavelengths. The convergence takes until $N = 7$ to produce a relative error of less than 5×10^{-2} and thus we accept the eight-mode approximation as converged. It is evident that the single-mode approximation is deficient in a number of ways: it is inaccurate both quantitatively and qualitatively, creating spurious characteristics, particularly for shorter wavenumbers. The only correct property retained is a decreasing tendency in $|R|$ as the incoming wavenumber decreases. However, by the four-mode approximation the spurious behaviour has been eliminated and the inaccuracies are mainly of a quantitative nature. The problems suffered by the single-mode approximation are attributed to the large jump that results from moving between free-surface and

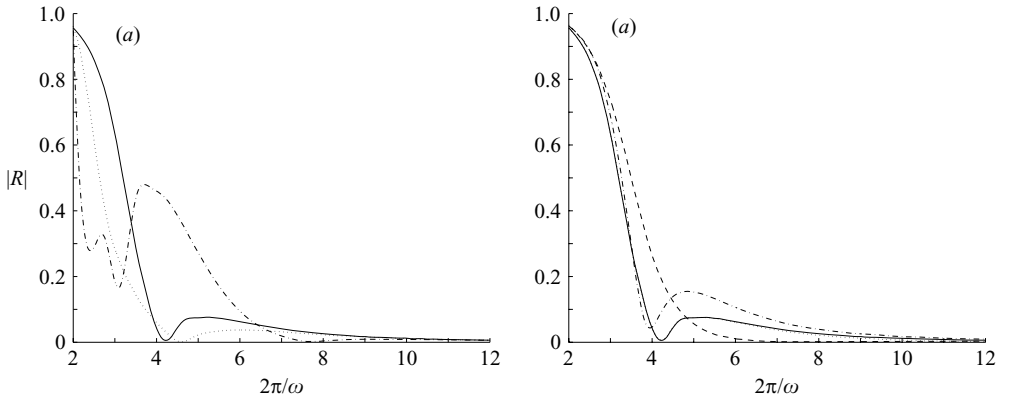

FIGURE 6. Partial ice-cover. No draught ($d=0$) with $D_0=1\,\mathrm{m}$, $l=10\,\mathrm{m}$ and $H_0=20\,\mathrm{m}$. (a) Convergence of MMA for a uniform floe. Dash-dot line ($N=0$), dotted line ($N=3$), solid line ($N=7$); (b) Converged approximations ($N=7$) for obstuctions of type (7.2) ($A_u=1\,\mathrm{m}$): solid line (uniform floe); dashed line (keel); dotted line (bed); dot-dash line (sail).

ice-covered states; despite this problem, it has been shown, in investigations that do not appear in this paper, that the convergence properties of the natural approximation outweigh benefits gained from using an approximation that maintains continuity. We must be aware that, unlike cases of continuous ice-cover, for partial ice-cover, a single natural-mode may not provide an accurate approximation.

Figure 6(b) provides a partial ice-cover counterpart to figure 4(b). Here, converged natural approximations to $|R|$ are given for the problem considered for figure 6(a) augmented by the addition of obstruction (7.2) where $A_u=1\,\mathrm{m}$, which takes three different positions (a sail, a keel and a bed variation). The converged ($N=7$) curve of the uniform floe over a flat bed shown in figure 6(a) is also included. For all three positions of the obstruction considered, eight modes are required to achieve $\epsilon_n<5\times10^{-2}$, which indicates that the primary difficulty is derived from the scattering at the vertical interfaces at the ends of the ice floe. This is corroborated by the shape of the curves that are dominated by the behaviour of the uniform floe. The most evident variations come in the sail and keel problems for $\pi/5<\omega<2\pi/3$. The sail impediment causes mainly quantitative changes, whereas the addition of a keel eliminates the minima around $\omega=\pi/2\,\mathrm{rad\,s^{-1}}$. This qualitative difference between the sail and keel problems contrasts with the findings for continuous ice-cover. Conversely, similarly to what was shown in the continuous ice-cover problem, the existence of a bed variation is of little consequence, here leading to a converged solution that is virtually indistinguishable from that of the uniform problem.

The geometrical configurations considered thus far, for cases of partial ice covering, have assumed no draught at the ends of the ice floes ($d\to0$ as $x\to0,l$) in order to isolate other effects. However, this has meant that we have been examining physically incorrect models of the ice floes. In figure 7, the effect of introducing a draught is considered, for a uniform floe of thickness $D=1\,\mathrm{m}$. The draught, d, must be calculated using Archimedes' principle, which implies that

$$\int_0^l \{\rho_i D(x)-\rho_w d(x)\}\,\mathrm{d}x=0.$$

For the uniform floe described, this dictates that $d(x)=0.9\,\mathrm{m}$ ($0<x<l$). Figure 7 displays converged natural approximations to the magnitude of the reduced

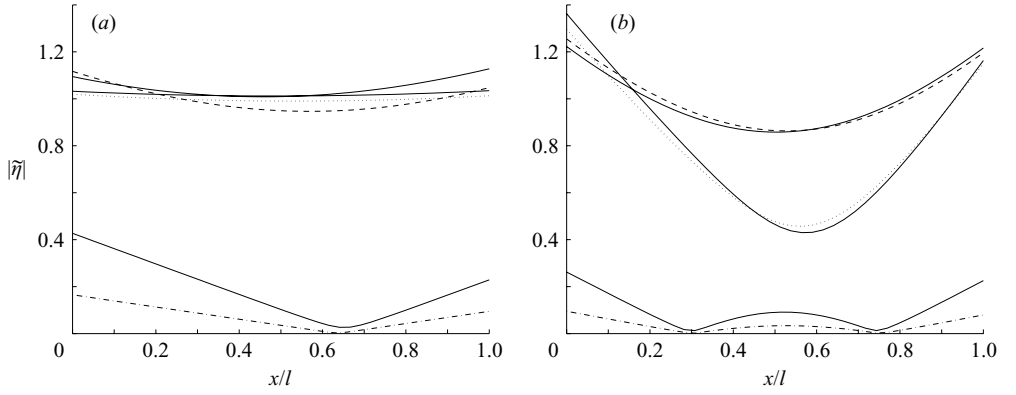

FIGURE 7. Partial ice-cover. Uniform floe ($D = 1\,\mathrm{m}$) over a constant bed depth ($H = 20\,\mathrm{m}$). Solid lines are for floes with no draught ($d = 0$) and broken lines are for floes including an Archimedean draught ($d = 0.9\,\mathrm{m}$): $\omega = \pi\,\mathrm{rad\,s^{-1}}$ (dot-dash); $\omega = \pi/3.449\,\mathrm{rad\,s^{-1}}$ (dashed); $\omega = \pi/6\,\mathrm{rad\,s^{-1}}$ (dotted). (*a*) $l = 10\,\mathrm{m}$; (*b*) $l = 50\,\mathrm{m}$.

displacement of the ice, $|\widetilde{\eta}|$, for three incident wavelengths and two differing floe lengths. It is noticeable that for the shorter incident waves, the ice is displaced with a smaller magnitude when an Archimedean draught is included but that as the incident wavelength increases, this feature diminishes. In all cases, the corresponding curves are qualitatively similar. We may also observe that as the incident wavelength decreases, the displacement decreases, which coincides with greater reflection (see, for instance, figure 6*b*). Finally, we note that, as we have previously found, a greater number of modes is required to achieve convergence as the incident wavelength decreases and, furthermore, the inclusion of an Archimedean draught also slightly slows convergence.

8. Conclusions

The formulation and implementation has been carried out of a general multi-mode approximation to the linearized motion of fluid bounded above by a floating elastic plate, which is currently used to describe ice floating on water, but has other applications. The user-defined modes contain the only appearance of the vertical coordinate in the approximation, and the application of a variational principle reduces the problem to one involving only the horizontal variables and thereby significantly reduces the difficulty to a level at which calculations involving varying ice thickness and undulating beds are feasible. The approximation, which is generated by an application of the Rayleigh–Ritz method, allows the solution of the full linear problem to be obtained to any degree of accuracy by selecting a suitably large trial space.

A particular (natural) trial space was suggested by PP, who investigated the single-mode version which the present MMA extends, in which modes corresponding to evanescent waves supplement the solitary mode that supports propagating waves. However, the inclusion of evanescent modes is compromised because the roots that determine their structure may bifurcate as one or more physical parameters vary, leading to the loss of required differentiability in the modes. It was noted that a two-fold linear dependence in the natural modes partially alleviates the problem caused by the bifurcations. In situations in which the problem presented by bifurcations persists, an alternative (hybrid) trial space that incorporates the first mode of the natural approximation, $\cosh k_0(z + h)$, together with finitely many members of the

Fourier modes $\cos l_n(z+h)$ for $n=1, \ldots,$ was used. This choice of hybrid modes is motivated by a wish to retain the original single-mode (to model the exact radiation conditions) and the fact that $\sigma_n \approx n\pi/H$. Of course, further alternative approximations are available; for instance, where a finite ice floe is surrounded by a free surface, a continuous expansion in the free-surface modes may be considered.

The jump conditions to be satisfied by the approximation, which are determined by the variational principle, also required extension to the multi-mode case. For partial ice-cover, this extension proved to be non-trivial as the matching conditions implemented by PP included a bias that could lead to inconsistencies if it were extended to multiple modes.

Results have been presented for a number of two-dimensional problems involving both complete and partial ice covering. Comparisons have been made to two sets of results obtained by previous authors using alternative methods. This helped to validate the MMA and also demonstrated rapid convergence of the natural approximation and excellent performance of single-mode approximations. Following this, problems were considered that use the ability of the MMA to handle fully variable geometry. A continuous ice-cover problem presented in PP was modified to include non-slow variations and solved using the alternative (hybrid) trial space. Despite the extreme variations in the geometry, the single-mode provided a good approximation and convergence was rapid. Through an example, it was shown that for all but long incoming waves, variations to the ice dominate over bed variations, in the sense that a greater amount of energy is reflected. Furthermore, it was seen that there is a marked similarity between solutions of keel and sail problems. For problems involving partial ice-cover it was shown that, as expected, the extra source of scattering produces effects that the MMA is required to resolve. Consequently, the single-mode $\cosh k_0(z+h)$ may produce an inaccurate approximation; however, on inclusion of evanescent modes these inaccuracies are quickly eliminated. The results presented indicated that the primary scattering effects may be attributed to the edges of the ice floe. Nevertheless, it was shown that ice variations (rather than bed variations), particularly a non-zero draught, can play a significant role.

There are many other problems involving varying ice thickness and undulating bed shapes that may be tackled with an MMA. Currently, work on the effect of ice with periodically varying thickness is in preparation, extending the free-surface counterparts studied by Porter & Porter (2002) and Porter & Chamberlain (1995), for which the existence of resonances is an issue. In three dimensions, investigations are being conducted into axisymmetric ice sheets in the vein of Peter *et al.* (2004).

Appendix

Here we give explicit formulae that are required in order to calculate the inner products appearing in the definition of the coefficients involved in the MMA (see § 4).

Let a general mode be defined as

$$w_i(x, y, z) \equiv W_i(D, h, d, z) = \cosh k_i(z+h),$$

where k_i (a root of the dispersion relation (2.2) if w_i is a natural mode) will be regarded as functions of the geometrical variables h, d and D. From now on, the notation

$$\mathrm{s}_i = \mathrm{s}_i(z) = \sinh k_i(z+h), \quad \mathrm{c}_i = \mathrm{c}_i(z) = \cosh k_i(z+h),$$

will be used for brevity.

For X (and/or Y) $= D, h$ or d, $(W_i, \partial_X W_j) = (\partial_X(k_j h))(\mathrm{c}_i, \mathrm{s}_j) + (\partial_X k_j)(z\mathrm{c}_i, \mathrm{s}_j)$, from which the expression

$$\begin{aligned}\partial_Y(W_i, \partial_X W_j) = {} & (\partial_Y \partial_X k_j)(\mathrm{c}_i, z\,\mathrm{s}_j) + (\partial_X k_j)\partial_Y(\mathrm{c}_i, z\,\mathrm{s}_j) \\ & + (\partial_Y \partial_X(k_j h))(\mathrm{c}_i, \mathrm{s}_j) + (\partial_X(k_j h))\partial_Y(\mathrm{c}_i, \mathrm{s}_j),\end{aligned}$$

is straightforward. Furthermore,

$$\begin{aligned}(\partial_Y W_i, \partial_X W_j) = {} & (\partial_Y k_i)(\partial_X k_j)(z\,\mathrm{s}_i, z\,\mathrm{s}_j) + (\partial_Y(k_i h))(\partial_X(k_j h))(\mathrm{s}_i, \mathrm{s}_j) \\ & + \{(\partial_Y(k_i h))(\partial_X k_j) + (\partial_Y k_i)(\partial_X(k_j h))\}(z\,\mathrm{s}_i, \mathrm{s}_j).\end{aligned}$$

The required inner-products of the hyperbolic functions can be calculated directly as

$$(\mathrm{c}_i, \mathrm{c}_j) = \begin{cases} \{k_i \mathrm{s}_i(-d)\mathrm{c}_j(-d) - k_j \mathrm{s}_j(-d)\mathrm{c}_i(-d)\}/\left(k_i^2 - k_j^2\right) & (i \neq j), \\ \{\mathrm{s}_i(-d)\mathrm{c}_i(-d) + k_i H\}/2k_i & (i = j), \end{cases}$$

$$(z\,\mathrm{c}_i, \mathrm{s}_j) = \begin{cases} -\{hk_j + d(k_i \mathrm{s}_i(-d)\mathrm{s}_j(-d) - k_j \mathrm{c}_i(-d)\mathrm{c}_j(-d)) \\ \quad + k_i(\mathrm{s}_i, \mathrm{s}_j) - k_j(\mathrm{c}_i, \mathrm{c}_j)\}/\left(k_i^2 - k_j^2\right) & (i \neq j), \\ \left\{h - d\left(\mathrm{c}_i^2(-d) + \mathrm{s}_i^2(-d)\right) - (\mathrm{c}_i, \mathrm{c}_i) - (\mathrm{s}_i, \mathrm{s}_i)\right\}/4k_i & (i = j), \end{cases}$$

$$\begin{aligned}(z\,\mathrm{s}_i, z\,\mathrm{s}_j) = {} & \{d^2(k_i \mathrm{c}_i(-d)\mathrm{s}_j(-d) - k_j \mathrm{s}_i(-d)\mathrm{c}_j(-d)) \\ & - 2(k_i(z\,\mathrm{c}_i, \mathrm{s}_j) - k_j(z\,\mathrm{s}_i, \mathrm{c}_j))\}/\left(k_i^2 - k_j^2\right) \quad (i \neq j),\end{aligned}$$

$$(z\,\mathrm{s}_i, z\,\mathrm{s}_i) = \{d^2 \mathrm{s}_i(-d)\mathrm{c}_i(-d) - 2(z\,\mathrm{c}_i, \mathrm{s}_i)\}/2k_i + (d^3 - h^3)/6,$$

with all other inner products following in a similar fashion. The derivitives required to evaluate $\partial_Y(W_i, \partial_X W_j)$ are

$$\begin{aligned}\partial_Y(\mathrm{c}_i, \mathrm{s}_j) = {} & (\partial_Y k_i)(z\,\mathrm{s}_i, \mathrm{s}_j) + (\partial_Y(k_i h))(\mathrm{s}_i, \mathrm{s}_j) + (\partial_Y k_j)(z\,\mathrm{c}_i, \mathrm{c}_j) \\ & + (\partial_Y(k_j h))(\mathrm{c}_i, \mathrm{c}_j) + [(\partial_Y z)\mathrm{c}_i \mathrm{s}_j]_{z=-h}^{-d},\end{aligned}$$

and

$$\begin{aligned}\partial_Y(z\,\mathrm{c}_i, \mathrm{s}_j) = {} & (\partial_Y k_i)(z\,\mathrm{s}_i, z\,\mathrm{s}_j) + (\partial_Y(k_i h))(z\,\mathrm{s}_i, \mathrm{s}_j) \\ & + (\partial_Y k_j)(z\,\mathrm{c}_i, z\mathrm{c}_j) + (\partial_Y(k_j h))(z\,\mathrm{c}_i, \mathrm{c}_j) + [(\partial_Y z)z\mathrm{c}_i \mathrm{s}_j]_{z=-h}^{-d}.\end{aligned}$$

Finally, various derivatives of the $k_i = k_i(D, h, d)$ appear in the expressions above. From here on, it is assumed that the k_i are roots of (2.2). (The derivatives of the l_i $(i = 1, \ldots)$ for the hybrid approximation are trivial.) Having found the k_i (see §4.1), analytic expressions for the derivatives may then be obtained in terms of the roots themselves. To carry this out, let the dispersion relation be expressed as

$$f(k, D)\tanh(kH) = \kappa : \quad f(k, D) = (1 - \alpha(D) + \beta(D)k^4)k.$$

The derivatives may then be deduced to be

$$\begin{aligned}E_i(\partial_D k_i) = {} & -(\partial_D f_i)\sinh(2k_i H), \quad E_i(\partial_d k_i) = 2f_i k_i, \quad E_i(\partial_h k_i) = -2f_i k_i, \\ E_i(\partial_D^2 k_i) = {} & -(\partial_k E_i)(\partial_D k_i)^2 - \left(\partial_D^2 f_i\right)\sinh(2k_i H) \\ & - 2(\partial_D k_i)\{(\partial_k \partial_D f_i)\sinh(2k_i H) + 2H(\partial_D f_i)\cosh^2(k_i H)\}, \\ E_i(\partial_h^2 k_i) = {} & -(\partial_k E_i)(\partial_h k_i)^2 - 4(\partial_h k_i)\{f_i + k_i(\partial_k f_i)\cosh^2(k_i H)\}, \\ E_i(\partial_d^2 k_i) = {} & -(\partial_k E_i)(\partial_d k_i)^2 + 4(\partial_d k_i)\{f_i + k_i(\partial_k f_i)\cosh^2(k_i H)\}, \\ E_i(\partial_D \partial_h k_i) = {} & -(\partial_k E_i)(\partial_D k_i)(\partial_h k_i) - 2k_i(\partial_D f_i) - 2(\partial_D k_i)\{f_i + k_i(\partial_k f_i)\} \\ & - (\partial_h k_i)\{(\partial_k \partial_D f_i)\sinh(2k_i H) + 2H(\partial_D f_i)\},\end{aligned}$$

$$E_i(\partial_D\partial_d k_i) = -(\partial_k E_i)(\partial_D k_i)(\partial_d k_i) + 2k_i(\partial_D f_i) + 2(\partial_D k_i)\{f_i + k_i(\partial_k f_i)\} - (\partial_d k_i)\{(\partial_k\partial_D f_i)\sinh(2k_i H) + 2H(\partial_D f_i)\},$$

and

$$E_i(\partial_d\partial_h k_i) = -(\partial_k E_i)(\partial_d k_i)(\partial_h k_i) + 2(\partial_h k_i)\{f_i + k_i(\partial_k f_i)\cosh(2k_i H)\} - 2(\partial_d k_i)\{f_i + k_i(\partial_k f_i)\},$$

where $f_i = f(k_i)$ and $E_i = E(k_i)$ such that

$$E(k) = \partial_k f(k)\sinh(2kH) + 2Hf(k),$$

with derivatives

$$\partial_k E = (\partial_k^2 f)\sinh(2kH) + 4H(\partial_k f)\cosh^2(kH),$$
$$\partial_k f = 1 - \alpha + 5\beta k^4, \quad \partial_D f = -D^{-1}k(\alpha - 3\beta k^4),$$

and

$$\partial_k^2 f = 20\beta k^3, \quad \partial_D^2 f = 6D^{-2}\beta k^5, \quad \partial_k\partial_D f = -D^{-1}(\alpha - 15\beta k^4).$$

It is clear that the function $E(k)$ vanishes only if $k = k_i$ is a multiple root of (2.2), which supports the comment concerning unboundedness made in § 4.1.

REFERENCES

Belibassakis, K. A. & Athanassoulis, G. A. 1999 A consistent coupled-mode theory for the propagation of small-amplitude water waves over variable bathymetry regions. *J. Fluid Mech.* **389**, 275–301.

Belibassakis, K. A. & Athanassoulis, G. A. 2005 A coupled-mode model for the hydroelastic analysis of large floating bodies over variable bathymetry regions. *J. Fluid Mech.* **531**, 221–249.

Balmforth N. J. & Craster R. V. 1999 Ocean waves and ice sheets. *J. Fluid Mech.* **395**, 89–124.

Chamberlain, P. G. & Porter, D. 1995 The modified mild-slope equation. *J. Fluid Mech.* **291**, 393–407.

Chamberlain, P. G. & Porter, D. 2006 Multi-mode approximations to wave scattering by an uneven bed. *J. Fluid Mech.* **556**, 421–441.

Evans, D. & Porter, R. 2003 Wave scattering by narrow cracks in ice sheets floating on water of finite depth. *J. Fluid Mech.* **484**, 143–165.

Evans, D. & Porter, R. 2006 Scattering of flexural waves by multiple narrow cracks in ice sheets floating on water. *Wave Motion* **43**, 425–443.

Evans, D. V. & Davies, T. V. 1968 Wave–ice interaction. Report no. 1313, Davidson Lab – Stevens Institute of Technology, New Jersey.

Fox, C. 2001 A scaling law for the flexural motion of floating ice. *Proc. IUTAM Symp. on Scaling Lams in Ice Mechanics and Ice Dynamics* (ed. J. P. Dempsey & H. H. Shen), pp. 135–148. Kluwer.

Fox, C. & Squire, V. A. 1994 On the oblique reflexion and transmission of ocean waves at shore fast sea ice. *Phil. Trans. Phys. Sci. Engng* **347**, 185–218.

Kagemoto, H. & Yue, D. K. P. 1986 Interactions among multiple threedimensional bodies in water waves: an exact algebraic method. *J. Fluid Mech.* **166**, 189–209.

Linton, C. M. & Chung, H. 2003 Reflection and transmission at the ocean/sea-ice boundary. *Wave Motion* **38**, 43–52.

Meylan, M. H. 2002 Wave response of an ice floe of arbitrary shape. *J. Geophys. Res.* **107**, doi: 10.1029/200JC000713.

Meylan, M. H. & Squire V. A. 1996 Response of a circular ice floe to ocean waves. *J. Geophys. Res.* **101**, 8869–8884.

Peter, M. A. & Meylan, M. H. 2004 Infinite depth interaction theory for arbitrary floating bodies applied to wave forcing of ice floes. *J. Fluid Mech.* **500**, 145–167.

Peter, M. A., Meylan, M. H. & Chung, H. 2004 Wave scattering by a circular elastic plate in water of finite depth: a closed form solution. *IJOPE* **14(2)**, 81–85.

Porter, D. & Chamberlain, P. G. 1995 Decomposition methods for wave scattering by topography with application to ripple beds. *Wave Motion* **22**, 201–214.

Porter, D. & Porter, R. 2002 Scattered and free waves over period beds. *J. Fluid Mech.* **483**, 129–163.

Porter, D. & Porter, R. 2004 Approximations to wave scattering by an ice sheet of variable thickness over undulating topography. *J. Fluid Mech.* **509**, 145–179.

Porter, D. & Staziker, D. J. 1995 Extensions of the mild-slope equation. *J. Fluid Mech.* **300**, 367–382.

Porter, R. 2004 Flexural-gravity wave diffraction by finite cracks of arbitrary shape in ice sheets *Proc. 19th Intl Workshop on Water Waves and Floating Bodies, Cortona, Italy*, March 2004.

Squire, V. A., Dugan, J. P., Wadhams, P., Rottier, P. J. & Liu, A. K. 1995 Of ocean waves and ice sheets. *Annu. Rev. Fluid Mech* **27**, 115–168.

Vaughan, G. L. & Squire, V. A. 2007 Scattering of ice-coupled waves by variable sea-ice terrain. *Ann. Glaciol.* **44**, 88–94.

Wang, C. M. & Meylan, M. H. 2002 The linear wave response of a floating thin plate on water of variable depth. *Appl. Ocean. Res.* **24**, 163–174.

Watanabe, E., Utsunomiya, T. & Wang, C. M. 2004 Hydroelastic analysis of pontoon-type VLFS: a lierature survey. *Engng Struct.* **26**, 245–256.

Williams, T. D. 2006 The scattering of flexural-gravity waves by irregularities in arctic and antarctic sea ice. PhD thesis, University of Otago, Dunedin, NZ.

Williams, T. D. & Squire, V. A. 2004 Oblique scattering of plane waves by heterogeneities in sea-ice. *Proc. R. Soc.Lond.* A **460**, 3469–3497.